Palaeogeography, Palaeoclimatology, Palaeoecology 440 (2015) 440–454

Contents lists available at ScienceDirect

Palaeogeography, Palaeoclimatology, Palaeoecology

journal homepage: www.elsevier.com/locate/palaeo

Redox conditions across the Cambrian–Ordovician boundary: Elemental and isotopic signatures retained in the GSSP carbonates

Karem Azmy [a,*], Brian Kendall [b], Uwe Brand [c], Svend Stouge [d], Gwyneth W. Gordon [e]

[a] Department of Earth Sciences, Memorial University of Newfoundland, St. John's, NL A1B 3X5, Canada
[b] Department of Earth and Environmental Sciences, University of Waterloo, Waterloo, ON N2L 3G1, Canada
[c] Department of Earth Sciences, Brock University, St. Catharines, ON L2S 3A1, Canada
[d] Geological Museum, University of Copenhagen, Øster Voldgade 5, DK-1350 Copenhagen K, Denmark
[e] School of Earth and Space Exploration, Arizona State University, Tempe, AZ 85287, USA

ARTICLE INFO

Article history:
Received 9 June 2015
Received in revised form 11 September 2015
Accepted 12 September 2015
Available online 25 September 2015

Keywords:
Cambrian–Ordovician GSSP
REE
Redox conditions
Organic C- and N-isotopes
U-isotopes
Western Newfoundland (Canada)

ABSTRACT

Lime mudstone samples (rhythmites) were collected at high resolution from outcrops of the Cambrian–Ordovician GSSP boundary section at Green Point (western Newfoundland, Canada). The sequence (~45 m-thick) consists of slope carbonates with alternating shale and siltstone interbeds, and it spans the boundary located between the Martin Point and Broom Point members of the Green Point Formation (Cow Head Group). Samples were extracted from micritic rhythmites by microdrilling and subsequently screened using petrographic and geochemical criteria to evaluate their degree of preservation. Although the $\delta^{13}C_{org}$ profile (−29.7 to −25.6‰ VPDB) shows insignificant variations, the TOC values (0.1 to 4.1%) exhibit a generally upward decreasing trend. A negative $\delta^{13}C_{carb}$ excursion, reflecting a sealevel rise, marks a geochemical anomaly that correlates with an increase in the N contents (0 to 2.9%) of organic matter and the $\delta^{15}N_{org}$ values (−0.6 to +6.0‰), which suggests a change to more reducing oceanic conditions. The U contents vary from 0.1 to 3.0 ppm and the $\delta^{238}U$ values (−0.97 to −0.18‰) generally decrease with the negative $\delta^{13}C_{carb}$ excursion. The U isotopic variations suggest a widespread increase in reducing conditions associated with sealevel rise during this interval. The investigated sedimentary rocks were slope carbonates where dysoxic conditions likely dominated throughout the entire section. Therefore, the changes in the TOC, N, $\delta^{15}N_{org}$, and $\delta^{238}U$ profiles across the boundary are not as sharp as would be expected by a local change from oxic shallow-water to dysoxic/anoxic deep-water settings.

1. Introduction

Chemostratigraphy has great potential to refine global stratigraphic correlations of sedimentary sequences. Preserved primary/near-primary stable isotope signatures in marine carbonates, which are associated with time events, provide high-resolution profiles for correlating sedimentary sequences from different depositional settings and paleocontinents (e.g., Veizer et al., 1999; Halverson et al., 2005; Immenhauser et al., 2008; Azmy et al., 2010). Earlier studies indicated that global sealevel changes along the eastern Laurentian margin around the Cambrian–Ordovician boundary influenced seawater redox conditions and organic productivity (e.g., Landing, 2012; Terfelt et al., 2012, 2014; Landing, 2013; Azmy et al., 2014). Those eustatic sealevel changes influenced the preservation of organic matter by reducing oceanic circulation and intensifying and thickening the mid-water dysoxic layer. The Cambrian–Ordovician boundary interval at Green Point may represent the late part of the so-called long-term "Hatch Hill dysoxic/anoxic interval" that began in the latest early Cambrian (Landing et al., 2002; Landing, 2012, 2013).

Sealevel changes also influence riverine inputs into the oceans and consequently the contents of trace elements in marine deposits (e.g., Wignall and Twitchett, 1996; Murphy et al., 2000; Arnaboldi and Meyers, 2007; Wignall et al., 2007; Piper and Calvert, 2009). The drop of oxygen level in seawater and the spread of dysoxic/anoxic conditions are known to be associated with global reduction of primary productivity and consequently the total organic carbon (TOC) contents and C- and N-isotope compositions of organic matter (e.g., Quan et al., 2008; Herrmann et al., 2012; Quan et al., 2013). Changes in global ocean redox conditions can be inferred from the $\delta^{238}U$ values of marine carbonates and organic-rich mudrocks (e.g., Weyer et al., 2008; Montoya-Pino et al., 2010; Brennecka et al., 2011; Asael et al., 2013; Kendall et al., 2013; Romaniello et al., 2013; Andersen et al., 2014; Dahl et al., 2014; Kendall et al., 2015). The Cambrian–Ordovician GSSP boundary section of Green Point (western Newfoundland, Canada) consists of slope deposits (rhythmites) of deep settings (James and Stevens, 1986) where dysoxic conditions are expected to be dominant (James and Stevens, 1986; Landing et al., 2002; Landing, 2012, 2013). The main objective of the current study is to investigate the C- and N-

* Corresponding author.
E-mail address: kazmy@mun.ca (K. Azmy).

http://dx.doi.org/10.1016/j.palaeo.2015.09.014
0031-0182/

isotope compositions of the organic matter in the lime mudstone rhythmites and the associated U-isotope compositions of those marine carbonates to understand changes in global ocean paleoredox conditions that occurred around that time interval.

2. Geologic setting

The Paleozoic sedimentary rocks of western Newfoundland in Canada (Fig. 1) were deposited on the eastern Laurentian margin (James et al., 1989). The Laurentian paleoplate developed by active rifting around 570 to 512 Ma (Cawood et al., 2001; Hibbard et al., 2007; Landing, 2007), and a pre-platform shelf formed and was covered by clastics (James et al., 1989). A major transgression flooded the Laurentian platform margin, which resulted in the accumulation of thick carbonate platform deposits (Wilson et al., 1992; Lavoie et al., 2013). Platform deposits were dominated by high-energy carbonates during the Middle and Late Cambrian (Port au Port Group, western Newfoundland, and evolved into low-energy carbonates of the St. George Group (western Newfoundland) during the Early to earliest Middle Ordovician (cf. Knight et al., 2007, 2008; Lavoie et al., 2013).

3. Litho- and biostratigraphy

Lithostratigraphy of the GSSP Cambrian–Ordovician boundary section in Green Point (western Newfoundland), which is a part of the Green Point Formation of the Cow Head Group (Fig. 2), has been studied and discussed in detail by James and Stevens (1986) and it will therefore be only summarized here. It consists of the uppermost Cambrian (Martin Point Member) and lowermost Ordovician (Broom Point Member), which are generally composed of dark gray to black fissile shale alternating with thin (~1 cm-thick) interbeds of ribbon limestone rhythmites. Siltstone interbeds (up to 1 cm thick) may co-occur with shales, and the limestone interbeds vary from isolated to combined layers of up to 20 cm. The conglomerate beds contain blocks of shallow water carbonates that were transported into the deep-water facies along the slope of the Laurentian margin (James and Stevens, 1986).

The Cambrian–Ordovician GSSP section at Green Point spans the *Cordylodus proavus* (Furongian, uppermost Cambrian) to the *Cordylodus angulatus* Zones (Tremadocian, Lower Ordovician). The Cambrian–Ordovician boundary is defined by the First Appearance Datum (FAD) of the conodont *Iapetognathus fluctivagus* (Barnes, 1988; Cooper et al., 2001). The current spike marking the Cambrian–Ordovician boundary in the GSSP section at Green Point is placed within Bed 23 slightly above the base of the negative $\delta^{13}C_{carb}$ excursion that marks a geochemical anomaly (Fig. 2; Azmy et al., 2014).

4. Methodology

Samples (Appendix 1, Fig. 2) were collected at high resolution (sampling intervals as small as 10 cm) from the Cambrian–Ordovician

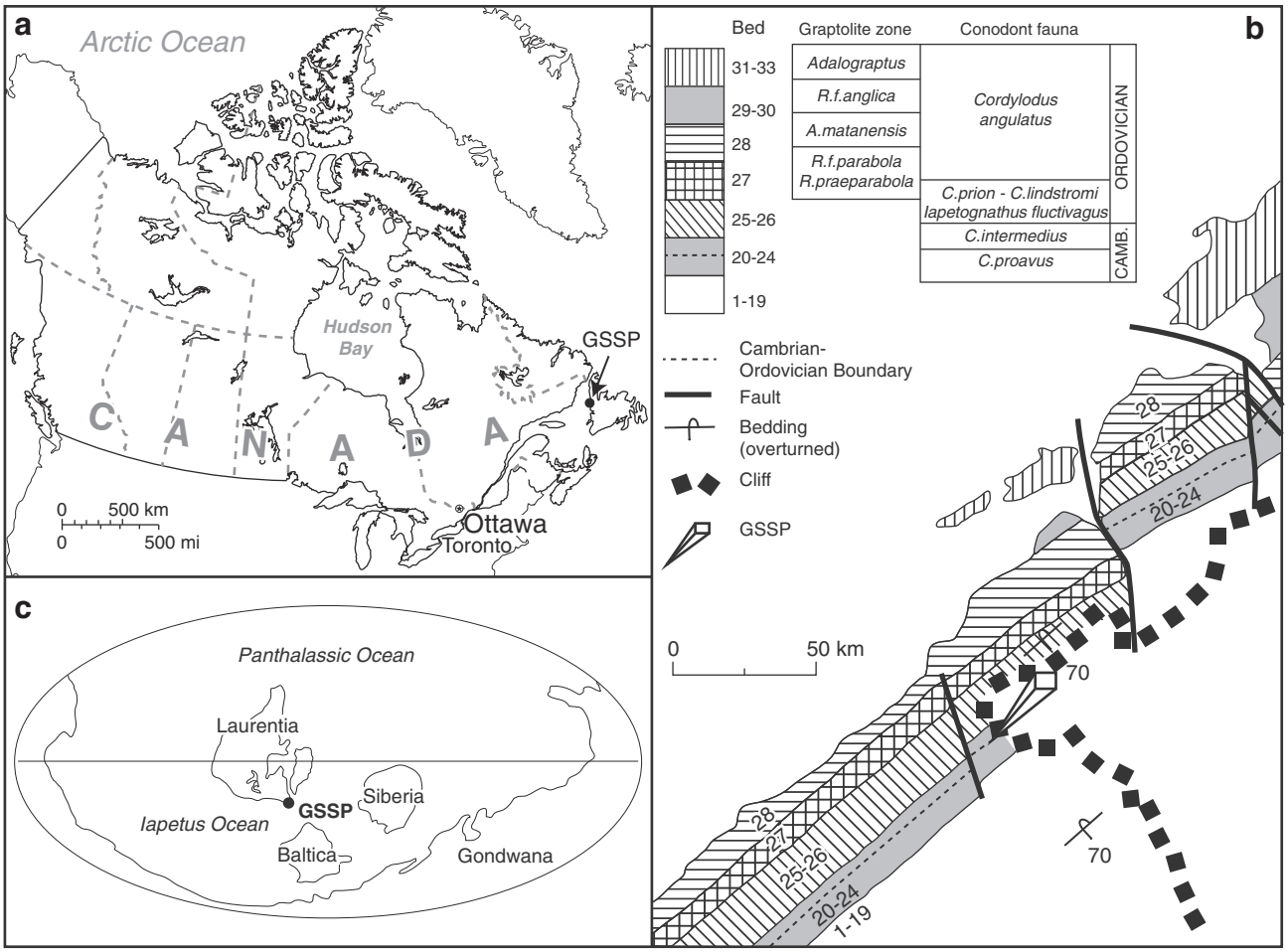

Fig. 1. Location map of Green Point, western Newfoundland, Canada showing (a) the location of the GSSP Cambrian–Ordovician boundary section in eastern Canada, and (b) the distribution of outcrops of the beds covering the boundary interval, and (c) the position of the GSSP on the paleomap during the Cambrian–Ordovician time interval.
(a) After Azmy et al. (2014). (b) Modified from Cooper et al. (2001). (c) Based on Scotese, C.R., 2002, PALEOMAP Project, http://www.scotese.com.

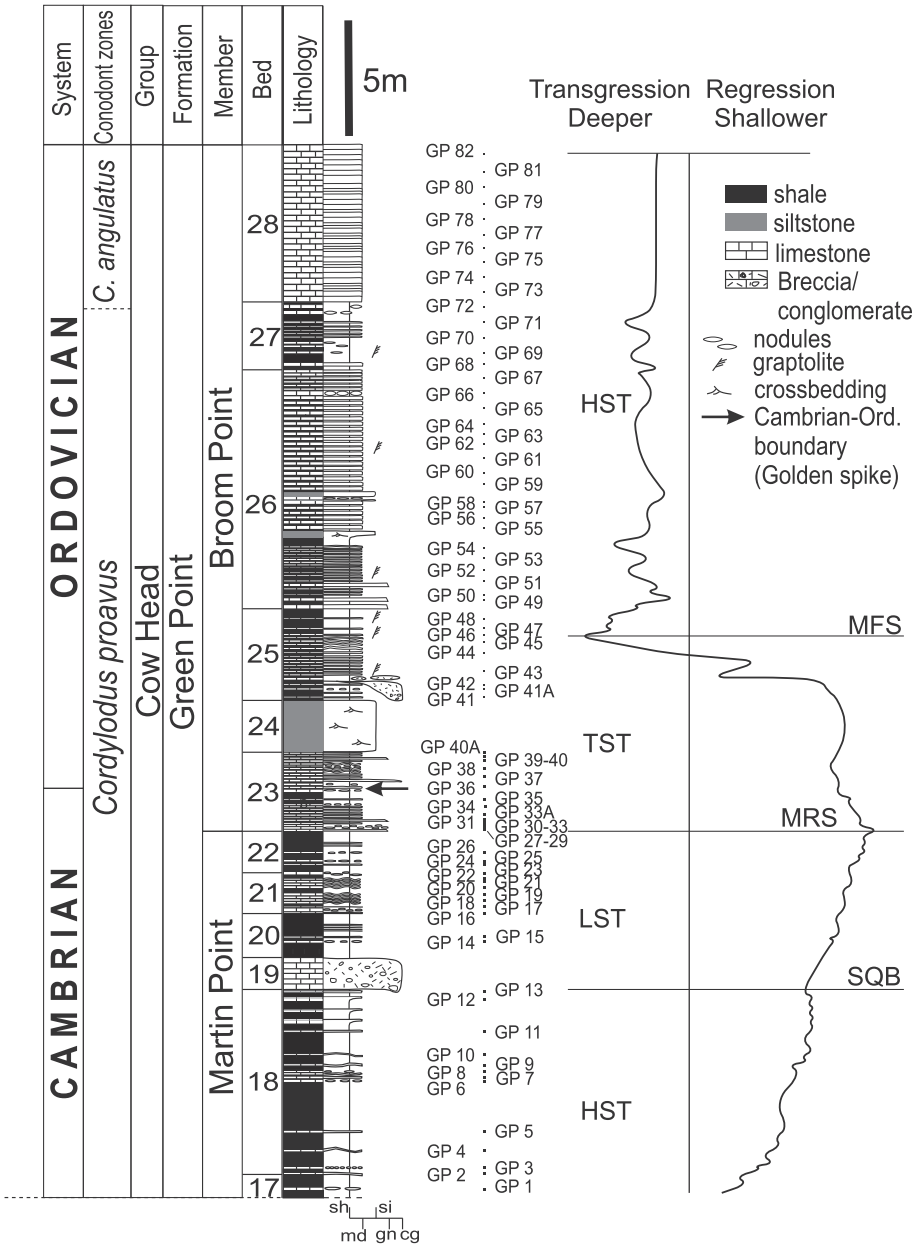

Fig. 2. Stratigraphic framework of the investigated Cambrian–Ordovician GSSP boundary section in western Newfoundland, Canada showing the detailed measured section with the positions of investigated samples and reconstructed sealevel variations across the boundary. Abbreviations as follows: HST — high stand systems tract, LST — low stand systems tract, TST — transgressive systems tract, MRS — maximum regressive surface, MFS — maximum flooding surface, and SQB — sequence boundary.
Conodont zonation after Landing et al. (2007).

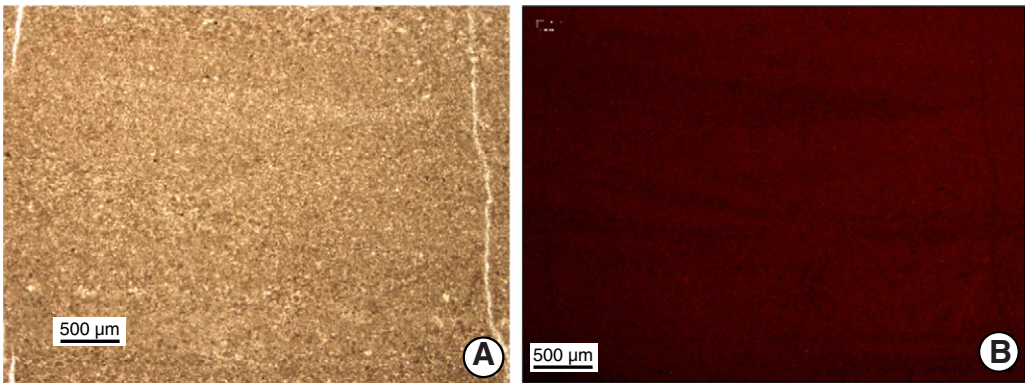

Fig. 3. Photomicrographs of the investigated carbonates showing (A) micritic lime mudstones (Sample GP 21) and (B) CL image of (A).

GSSP boundary section (49° 40′ 51″ N; 57° 57′ 36″ W) at Green Point, western Newfoundland (Fig. 1). They were taken from the laminated lime mudstone rhythmites to avoid allochthonous clasts (Fig. 3A, B). Thin sections of samples were examined petrographically with a polarizing microscope (cf. Azmy et al., 2014) and stained with Alizarin Red-S and potassium ferricyanide solutions (Dickson, 1966). Cathodoluminescence (CL) observations were performed using a Technosyn 8200 MKII cold cathode instrument operated at 8 kV accelerating voltage and 0.7 mA current.

A mirror-image slab of each thin section was also prepared and polished for microsampling. Polished slabs were washed with deionized water and dried overnight at 50 °C prior to isolating the finest grained micritic lime mudstone free of secondary cements. Up to 10 g of powder was extracted from the finest grain material.

For elemental analyses, a subset of sample powder was digested in 5% (v/v) acetic acid for 70–80 min and analyzed for major, minor and rare earth elements (REEs) using an Elan DRC II ICP-MS (Perkin Elmer SCIEX) at Memorial University of Newfoundland. International (DLS-88a and CCH-1) and internal standards were utilized to normalize the results. The relative uncertainties of these measurements are better than 5%, and results are normalized to a 100% carbonate basis.

Organic carbon- and nitrogen-isotope ratios were measured on isolated kerogen after repeated treatment with pure concentrated hydrochloric acid at the isotope laboratory of Memorial University of Newfoundland, using a Carlo Erba Elemental Analyzer coupled to a ThermoFinnigan DELTA V plus isotope ratio mass spectrometer in a stream of helium, where the gas was ionized and measured for isotope ratios. The results were normalized to the standards IAEA-CH-6 ($\delta^{13}C = -10.43‰$ VPDB), NBS18 ($\delta^{13}C = -5.04‰$ VPDB), USGS24 ($\delta^{13}C = -15.99‰$ VPDB), IAEA-N-1 ($\delta^{15}N = 0.43‰$ air), and IAEA-N-2 ($\delta^{15}N = 20.32‰$ air). The uncertainty calculated from repeated measurements was ~0.2‰.

Uranium isotope measurements were carried out at the W.M. Keck Foundation Laboratory for Environmental Biogeochemistry, School of Earth and Space Exploration, Arizona State University. Between 2 and 9 g of powdered sample was first ashed at 750 °C to calcinate the carbonate matrix, thus destroying all organic matter (Romaniello et al., 2013). A cold leach with dilute 1 M HCl and then 1 M HNO_3 was used to extract authigenic U from the samples while minimizing inclusion of detrital material. A portion of the sample solution corresponding to approximately 500 ng of U was equilibrated with a double spike (^{233}U–^{236}U; IRMM3636; Verbruggen et al., 2008; Romaniello et al., 2013) by reacting the sample-spike mixture in concentrated HNO_3 and HCl. The sample-spike mixture was passed through UTEVA resin to separate U (Weyer et al., 2008). After column chemistry, samples were reacted with a HNO_3–H_2O_2 mixture to destroy residual organic material from the UTEVA resin (Romaniello et al., 2013). Samples were re-dissolved in 2% HNO_3 and analyzed on a multi-collector inductively coupled plasma mass spectrometer (MC-ICP-MS; Thermo Scientific Neptune) using an ESI Apex desolvating nebulizer (Kendall et al., 2013; Romaniello et al., 2013). The U concentration of each sample was calculated using double spike isotope dilution analysis. Sample $\delta^{238}U$ was reported relative to the CRM 145 standard as follows (Romaniello et al., 2013):

$$\delta^{238}U(‰) = \left[\left(^{238/235}U_{sample}/^{238/235}U_{CRM\ 145}\right)-1\right] \times 1000.$$

Instrument accuracy and precision were verified by analysis of the secondary standards SRM 950a and CRM 129a. During the course of this study, the average $\delta^{238}U$ for SRM 950a and CRM 129a was 0.01 ± 0.11‰ (2SD, n = 4) and −1.71 ± 0.08‰ (2SD, n = 16), respectively. This is in excellent agreement with previous studies that determined the values of SRM 950a and CRM 145 to be statistically indistinguishable (Weyer et al., 2008; Condon et al., 2010; Kendall et al., 2013), and with previous measurements of CRM 129a (Brennecka et al., 2011; Kendall et al., 2013). Based on the reproducibility of the more frequently measured CRM 129a standard, the 2σ uncertainty of a sample measured in the current study is the 2σ uncertainty of sample replicate measurements or 0.08‰, whichever is greater. Other recent studies using the Thermo Scientific Neptune at Arizona State University report similar uncertainties for CRM 129a (Kendall et al., 2013, 2015). Most samples were run at least in duplicate during different mass spectrometry sessions, with the exception of a few samples for which inadequate solution was available. In addition, $\delta^{234}U$ was measured simultaneously with $\delta^{238}U$ using the procedure of Romaniello et al. (2013), and is reported as:

$$\delta^{234}U(‰) = \left[\left(^{234/238}U_{sample}/^{234/238}U_{CRM\ 145}\right)-1\right] \times 1000.$$

Relative to secular equilibrium, CRM 145 has a value of −36‰ to −37‰ (Andersen et al., 2004). The value of CRM 145 was set to −36.7‰ (Romaniello et al., 2013). As the samples analyzed in this study are from the Cambrian–Ordovician GSSP, the U isotope systematics should be in secular equilibrium provided that samples have not been recently disturbed during the past ~2 Ma, and thus should have $\delta^{234}U$ values close to 0‰. Full powder replicates for three samples (GP 2, GP 28, and GP 59) demonstrate excellent reproducibility for both $\delta^{238}U$ and $\delta^{234}U$.

5. Results

Petrographic examinations indicated that the examined material was dominantly micritic carbonate rhythmites with <1% disseminated microrhombic pyrite of most likely microbial origin and an earlier study (Azmy et al., 2014) indicated that there is a negative $\delta^{13}C_{carb}$ excursion, which starts at a stratigraphic level slightly below the suggested biostratigraphic boundary (Figs. 2 and 4). Table 1 summarizes the statistics of geochemical results of the GSSP Cambrian–Ordovician boundary carbonate rhythmites. The total organic content (TOC) varies between 0.1 and 4.1% and the $\delta^{13}C_{org}$ signatures vary from −25.6 to −29.7‰ (VPDB). Mean values of $\delta^{13}C_{org}$ in the beds below the $\delta^{13}C_{carb}$ excursion and those correlated with the excursion (cf. Azmy et al., 2014) are almost the same (−27.2 ± 1.2‰ and −27.8 ± 1.1‰ VPDB, respectively; Table 1). By contrast, the mean TOC contents are lower in the beds correlated with the $\delta^{13}C_{carb}$ excursion (0.6 ± 0.5 vs. 1.7 ± 0.9 wt.%, Table 1). The TOC contents are generally within the range documented for shales from around the Cambrian–Ordovician boundary in many locations in western Newfoundland (0.6 to 5.2 wt.%; Weaver and Macko, 1988). Similarly, their $\delta^{13}C_{org}$ values are consistent with those documented for crude oil seeps from the same shales (−28.2 to −33.0‰; Weaver and Macko, 1988).

The $\delta^{15}N_{org}$ signatures range from −0.6 to +6.0‰ (Table 1) where the most depleted values are lower than those documented for present-day Black Sea sediments (~3‰, Fry et al., 1991; Çoban-Yıldız et al., 2006) and modern marine biomass and nitrates (~5‰, Galbraith et al., 2008). The GSSP $\delta^{15}N_{org}$ values are also within the range documented for kerogen extracted from shales of the same age in western Newfoundland (−1.2 to −7.1‰; Weaver and Macko, 1988). The mean $\delta^{15}N$ values (1.2 ± 1.2‰) of the carbonate beds below the geochemical anomaly, marked by the start of the negative $\delta^{13}C_{carb}$ excursion (Azmy et al., 2014), are generally lower than that of their counterparts above the anomaly (2.8 ± 1.5‰, Table 1 and Fig. 4).

The U concentrations vary between 0.1 and 4.3 ppm (Table 1). The $\delta^{238}U$ values vary between −0.18 and −0.97‰ and there is a

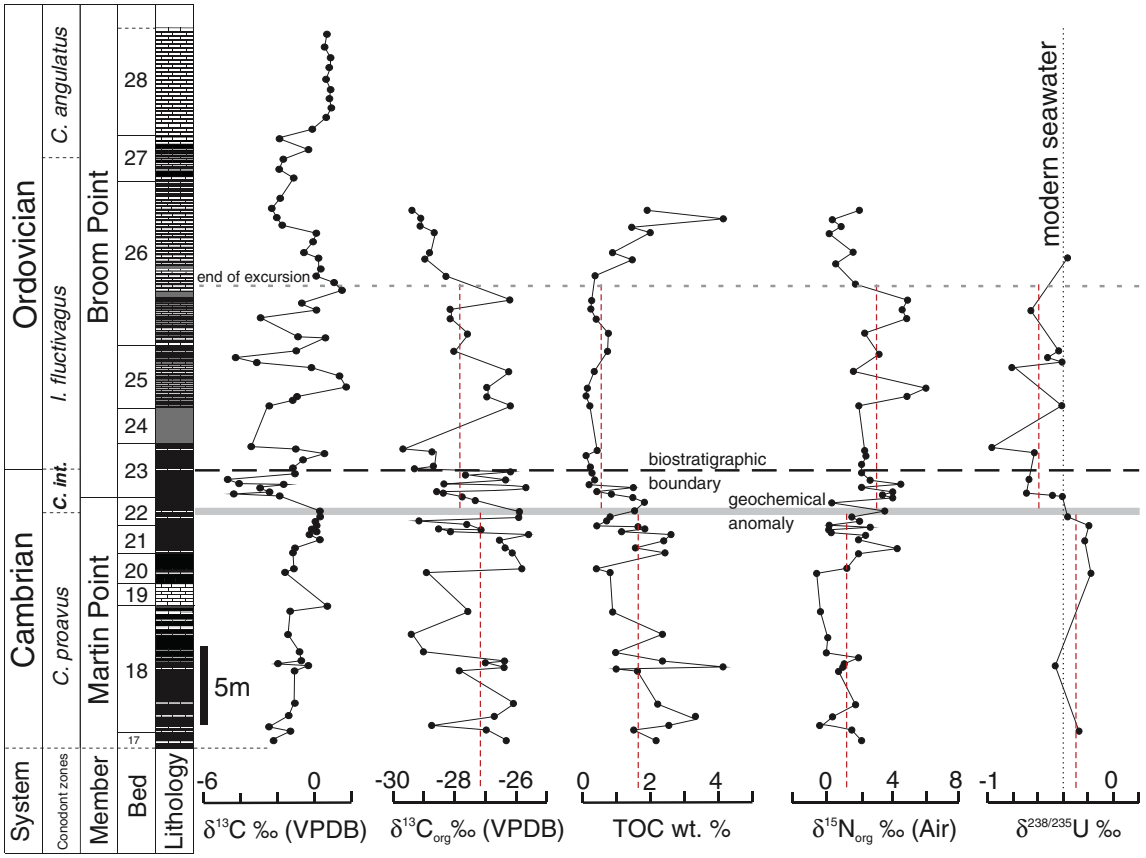

Fig. 4. The $\delta^{13}C_{org}$, TOC, $\delta^{15}N_{org}$, and $\delta^{238}U$ profiles of lime mudstone rhythmites across the Cambrian–Ordovician GSSP boundary section. The solid gray line refers to the level of the geochemical anomaly recorded by Azmy et al. (2014) and the dashed black line marks the current position of the Cambrian–Ordovician boundary defined by the FAD of *I. fluctivagus* (Cooper et al., 2001). The dashed vertical red lines are the mean values below and above the geochemical anomaly levels.
The $\delta^{13}C_{carb}$ is reproduced from Azmy et al. (2014).

noticeable decrease from -0.28 ± 0.11‰ below the geochemical anomaly level to -0.58 ± 0.18‰ during the negative $\delta^{13}C_{carb}$ excursion (Fig. 4 and Table 1). With respect to $\delta^{234}U$, most samples fall within 15‰ of secular equilibrium. There is no correlation between $\delta^{234}U$ and $\delta^{238}U$ or between U concentrations and $\delta^{234}U$ ($R^2 < 0.1$). A moderate correlation occurs between U concentrations and $\delta^{238}U$ ($R^2 = 0.47$).

6. Discussion

6.1. Evaluation of sample preservation

6.1.1. Petrographic preservation

Petrography and preservation of micritic fabric of the investigated samples have been discussed in detail by Azmy et al. (2014) and are

Table 1
Summary of statistics of GSSP geochemical results.

		$\delta^{13}C_{org}$	% TOC	$\delta^{15}N_{air}$	% N	$\delta^{238}U$	U (ppm)	Th/U
n	Above geochem anomaly (Sample Gp26)	26	26	27	26	13	36	15
Average		−27.8	0.6	2.8	0.33	−0.58	0.7	0.7
Stdev		1.1	0.5	1.5	0.62	0.18	0.7	0.5
Max		−25.7	2.1	6.0	2.91	−0.37	3.0	1.7
Min		−29.7	0.1	0.1	0.00	−0.97	0.1	0.2
n	Below geochem anomaly (Sample Gp26)	25	25	25	25	6	26	24
Average		−27.2	1.7	1.2	0.01	−0.28	1.2	0.5
Stdev		1.2	0.9	1.2	0.01	0.11	0.6	0.4
Max		−25.6	4.1	4.3	0.06	−0.18	2.7	1.7
Min		−29.4	0.4	−0.6	0.00	−0.46	0.3	0.1
n	Entire section	51	51	52	51	19	62	39
Average		−27.5	1.1	2.0	0.17	−0.47	1.0	0.6
Stdev		1.2	1.0	1.6	0.47	0.21	0.8	0.4
Max		−25.6	4.1	6.0	2.91	−0.18	4.3	1.7
Min		−29.7	0.1	−0.6	0.00	−0.97	0.1	0.1

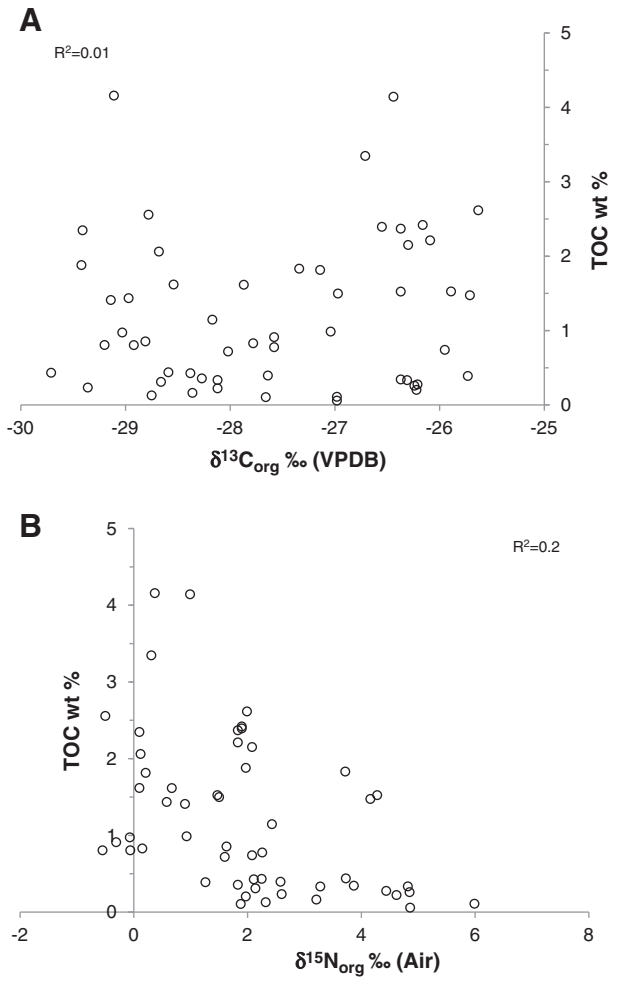

Fig. 5. Scatter diagrams of (A) $\delta^{13}C_{org}$ vs. TOC and (B) $\delta^{15}N_{org}$ vs. TOC showing insignificant correlations. Detail in text.

summarized below. Except for two samples around the top of Bed 18 in the middle of the Martin Point Member that contained laminae of argillaceous carbonates (Samples GP11 and GP12, Appendix 1), the Green Point Formation at the Cambrian–Ordovician GSSP is dominated by fabric retentive lime mudstones (rhythmites of micritic to near-micritic grain size) with insignificant recrystallization (Fig. 3A) and no- to dull luminescence under cold cathodoluminoscope (Fig. 3B). These observations suggest a high degree of petrographic preservation (Azmy et al., 2014). Luminescence in carbonates is mainly activated by high concentrations of Mn and quenched by high concentrations of Fe (Machel and Burton, 1991). Although dull luminescence may indicate relatively good preservation of geochemical signatures, altered carbonates may still exhibit no luminescence due to high-Fe content (Rush and Chafetz, 1990). Therefore, cathodoluminescence is a single evaluation tool that has to be confirmed by other screening tests (Brand et al., 2011).

6.1.2. Geochemical preservation

Preservation of the elemental geochemical signatures in the investigated samples has been discussed in detail by Azmy et al. (2014). The progressive burial of sediments during the diagenetic history of basins is associated with an increase in temperature (>50 °C), which leads to a thermal degradation of the organic matter and a decrease in the TOC that becomes isotopically heavier as ^{12}C-enriched organic compounds are released (e.g., Popp et al., 1997; Faure and Mensing, 2005). The insignificant correlation ($R^2 = 0.01$) between the $\delta^{13}C_{org}$ and TOC wt.% values (Fig. 5A) argues against significant bio- and thermal degradation and is consistent with preservation of the micritic texture, thus suggesting a high degree of preservation of the $\delta^{13}C_{org}$ signatures. This is consistent with the poor correlation between the $\delta^{15}N_{org}$ and TOC wt.% values (Fig. 5B; e.g., Yamaguchi et al., 2010), which also supports the preservation of the $\delta^{15}N_{org}$ signatures. Limited deviation in $\delta^{234}U$ from secular equilibrium, together with the absence of a correlation between $\delta^{234}U$ and $\delta^{238}U$, points to minimal modification of $\delta^{238}U$ signatures by recent fluid flow during the past ~2 Ma. Also, the insignificant correlations ($R^2 < 0.1$) between elements known to be enriched in crustal clastic rocks, such as Al and Ti, with the $\delta^{238}U$ values (Appendix 1) argue for the primarily authigenic nature of those isotope signatures in the carbonates and minimal overprint by silicate inclusions.

6.2. Elemental variations

Variations in sealevel, particularly those related to time events, are generally associated with changes in trace and rare earth element (REE) concentrations in sediments due to inputs of terrestrial material and/or changes in redox conditions (e.g., Wignall and Twitchett, 1996; Murphy et al., 2000; Kimura et al., 2005; Arnaboldi and Meyers, 2007; Wignall et al., 2007; Piper and Calvert, 2009; Śliwiński et al., 2010; Dickson et al., 2011). Therefore, major $\delta^{13}C_{carb}$ shifts of remarkable time events reflect relative changes in organic productivity and paleoredox conditions (e.g., Azmy et al., 2014). An earlier detailed study of the $\delta^{13}C_{carb}$ profile of the GSSP Cambrian–Ordovician boundary at Green Point by Azmy et al. (2014) documented a significant negative excursion (~6‰) near the top of Bed 22 (Fig. 4). Phosphorous, Cu, and Ni have been utilized as proxies for bioproductivity and V, Cr, Co, Mo, and Th/U for paleoredox (e.g., Hatch and Leventhal, 1992; Wignall and Twitchett, 1996; Falkowski, 2004; Morel et al., 2004; Azmy et al., 2012). However, the investigated boundary section at Green Point consists of carbonates deemed to be deposited in slope settings (James and Stevens, 1986) where the abundance of biota below the photic zone is generally low, particularly during the Early Paleozoic, compared with their shallow water counterparts. Also, many of those proxies were formulated based on applications to shales and sapropels that have different mineralogical and chemical compositions from those of carbonates (e.g., Hatch and Leventhal, 1992; Arnaboldi and Meyers, 2007; Zhou et al., 2012). Therefore, the application of elemental proxies to slope carbonates has to be done with caution since not all proxies are expected to show consistent responses similar to those observed in shallow shelf sedimentary rocks.

A few samples in the Green Point section exhibit a significant enrichment in P (up to 7914 ppm, Samples GP 27 and 28, Appendix 1), which is also coupled with significant enrichment in $\sum$REE (267 ppm). No other correlated consistent enrichment in other proxies such as V, Cr, Co, Ni, Cu, or Mo has been detected at the boundary level (Appendix 1) since their concentrations are below detection limits (e.g., Co, Ni, Cu) and most of those of V and Cr are below 5 ppm except for a few values (Appendix 1). Although enrichment in P could be attributed to an increase in primary productivity possibly due to increase in terrestrial input of organic matter and/or nutrient input from upwelling currents (e.g., Azmy et al., 2011), the high-P samples in the investigated section were peloidal algal mud to grainstones that contain phosphatic laminated algae or aggregates, which most likely resulted in the high P contents (Azmy et al., 2014). Those few high P samples have also high total REE ($\sum$REE) contents (Appendix 1) where REE are known to be enriched particularly in biogenic phosphates (e.g., Lécuyer et al., 1998). The scarcity of high P samples is also consistent with the expected low density of terrestrial plants (source of organic matter) during the late Cambrian to early Ordovician (e.g., Davies and Gibling, 2010).

High Al and Si values around the top of Bed 18 in the middle of the Martin Point Member are associated with argillaceous carbonates (Samples GP11 and GP12, Appendix 1) and do not correlate with P or $\sum$REE

contents. These variations may reflect an abrupt input of siliciclastics into the slope carbonates possibly due to short-term turbidity particularly with the lack of correlation with a time event or influence on the $\delta^{13}C$ values (Azmy et al., 2014).

Levels of oxygen in the water column influence the oxidation state of redox-sensitive elements and selectively control their solubility in seawater and consequently their degree of enrichment in marine sediments (e.g., Wignall and Twitchett, 1996; Kimura et al., 2005; Tribovillard et al., 2006; Arnaboldi and Meyers, 2007; Wignall et al., 2007). In oxidizing environments, uranium ions maintain the higher oxidation state (U^{+6}) and form uranyl carbonate, which is soluble in water whereas in reducing conditions, they retain the lower oxidation state (U^{+4}) and form the insoluble uranous fluoride which is trapped into marine carbonates (Wignall and Twitchett, 1996). In contrast, thorium is not affected by redox conditions in the water column and occurs permanently in the insoluble Th^{+4} state. Accordingly, sediments of anoxic environments are richer in uranium and have lower Th/U than those of oxic environments. Therefore, the Th/U ratio has been used as a proxy for environmental redox conditions, with ratios <2 in anoxic marine sediments and >2 in oxic sediments (cf. Wignall and Twitchett, 1996). The Th/U values of the Green Point carbonates are <2 throughout the entire boundary section, thus reflecting reducing conditions. However, the Y/Ho (proxy of preservation of REE composition of carbonates; Webb and Kamber, 2000) values of the Green Point carbonates (34 ± 5) are lower than those suggested for Holocene marine carbonates (≥50, Webb and Kamber, 2000; Azmy et al., 2014), which implies minor alteration of the elemental geochemical signatures even at low water/rock ratios. Therefore, the interpretation of the Th/U values has to be taken with some caution, particularly when ratios of <2 are associated with occurrences of phosphatic algae that cannot tolerate reducing conditions (Azmy et al., 2014).

Cerium anomalies provide complementary information on local redox conditions. The Ce/Ce* values of the Green Point carbonates are higher than the range documented for Holocene microbialites of well-oxygenated shallow water settings, and thus record relatively reducing conditions (Webb and Kamber, 2000; Fig. 6). However, a small number of values falls within the Holocene Ce/Ce* range of shallow water microbialites although they have lower Y/Ho ratios. The relatively higher Ce/Ce* values are expected for slope carbonates because Ce is oxidized in shallow oxic water into CeO_2, which is scavenged by organic matter leaving shallow water depleted in Ce.

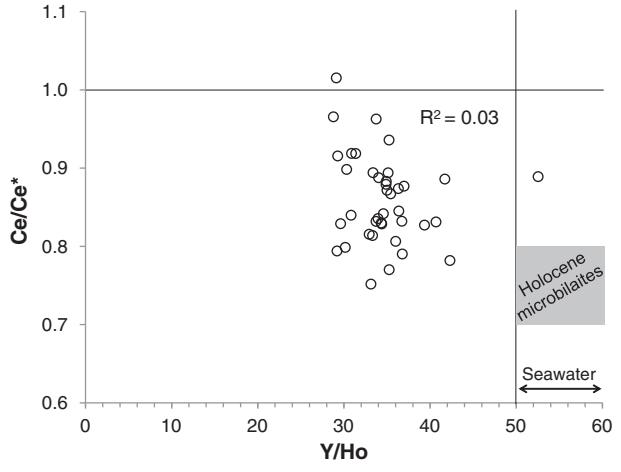

Fig. 6. Scatter diagram showing the correlations of Ce/Ce* vs. Y/Ho for the investigated carbonates. Ce_{SN} $[(Ce/Ce^*)_{SN} = Ce_{SN}/(0.5La_{SN} + 0.5Pr_{SN})]$ and La_{SN} $[(Pr/Pr^*)_{SN} = Pr_{SN}/(0.5Ce_{SN} + 0.5Nd_{SN})]$ anomalies were calculated with the equations of Bau and Dulski (1996). The gray square represents the composition of Holocene microbialites (Webb and Kamber, 2000).

Shallow-water carbonates thus have lower Ce/Ce* values than those of relatively deeper water settings with less oxygen (e.g., Alibo and Nozaki, 1999). The generally high Ce/Ce* values (0.86 ± 0.06) of the Green Point carbonates are <1 and they therefore possibly reflect suboxic/dysoxic conditions rather than anoxia (Webb and Kamber, 2000); a condition reconcilable with the low Th/U ratios (<2) and the occurrence of phosphatic algae.

The low pyrite content in the GSSP boundary section (<1%) supports dysoxic rather than anoxic conditions in local bottom waters. This suggests that the drop in the oxygen level led to reduction in primary productivity but was not severe enough to reach extinction levels, which is consistent with the paleontological evidence (cf. Cooper et al., 2001; Terfelt et al., 2014).

6.3. Organic C- and N-isotopes

The $\delta^{13}C_{org}$ profile of the GSSP at Green Point shows wide variations of up to 4‰ (between ~−29.7 and −25.6‰ VPDB; Table 1) before the $\delta^{13}C_{carb}$ excursion (Fig. 4). The width of the variations decreases considerably through the upper part of the excursion although the $\delta^{13}C_{org}$ profile generally exhibits a parallel trend to its $\delta^{13}C_{carb}$ counterpart particularly at the excursion interval. However, the TOC contents decrease noticeably with the $\delta^{13}C_{carb}$ excursion (Fig. 4) and their profile starts to increase again at the level above the $\delta^{13}C_{carb}$ shift. The decline in TOC content during the excursion suggests a drop of marine organic productivity particularly for sediments of slope settings where oxidation of organic matter is unlikely. The lack of significant correlation between the $\delta^{13}C_{org}$ and TOC values strongly supports the preservation of their signatures (Fig. 5A) and the correlation of the $\delta^{13}C_{carb}$ excursion with lower TOC contents (Fig. 4), compared with those in the lower section, suggests that a sealevel rise led to relative reduction in organic productivity at the Cambrian–Ordovician boundary (Lehnert et al., 2005).

The investigated carbonates have low C/N ratios of ≪10 (Table 1 and Appendix 1), which implies insignificant contribution from terrestrial plants and is consistent with the low diversity of land plants during the earliest Phanerozoic (e.g., Meyers, 1994; Theissen et al., 2003). The mean values of N contents show an increase in the beds above the geochemical anomaly level (Table 1) in association with the negative $\delta^{13}C_{carb}$. The $\delta^{15}N_{org}$ profile of the GSSP section also exhibits relative enrichment in ^{15}N (~1.6‰ higher) in the beds correlated with the $\delta^{13}C_{carb}$ excursion (Table 1 and Fig. 4), which is consistent with a sealevel rise during the Cambrian–Ordovician boundary and with enhanced fractionation due to denitrification (e.g., Quan et al., 2013). The generally low $\delta^{15}N$ values (2.0 ± 1.6‰) through the GSSP are comparable with those documented for modern Black Sea sediments (~3‰), and thus suggest a period of relative stagnation and low primary productivity dominated by suboxic/dysoxic to anoxic conditions (e.g., Quan et al., 2008). This is consistent with the conclusions from the Th/U (<2) values (Appendix 1) and with the Ce/Ce* ratios (near unity) that vary between 0.8 and 1.0 (Fig. 6, Azmy et al., 2014). Despite the isotopic enrichment during active denitrification, the investigated organic matter has $\delta^{15}N$ values depleted relative to modern phytoplankton (~2 to 7‰, Faure and Mensing, 2005), thus suggesting an influence by N_2-fixing bacteria rather than terrestrial inputs, which is also consistent with the low abundance of terrestrial plants around the time of the early Paleozoic (e.g., Davies and Gibling, 2010).

6.4. U-isotopes

Uranium concentrations have been found to vary from an average of ~1.5 ppm in modern shallow marine biogenic carbonates to an average of ~4.1 ppm in bulk sediment counterparts (Romaniello et al., 2013). The average concentration of U in the GSSP lime mudstones (1.0 ± 0.8 ppm, Table 1) is generally lower than that of modern marine carbonates but there is no clear evidence or a reason to expect depletion of U concentrations in the GSSP carbonates by diagenesis. The near-micritic

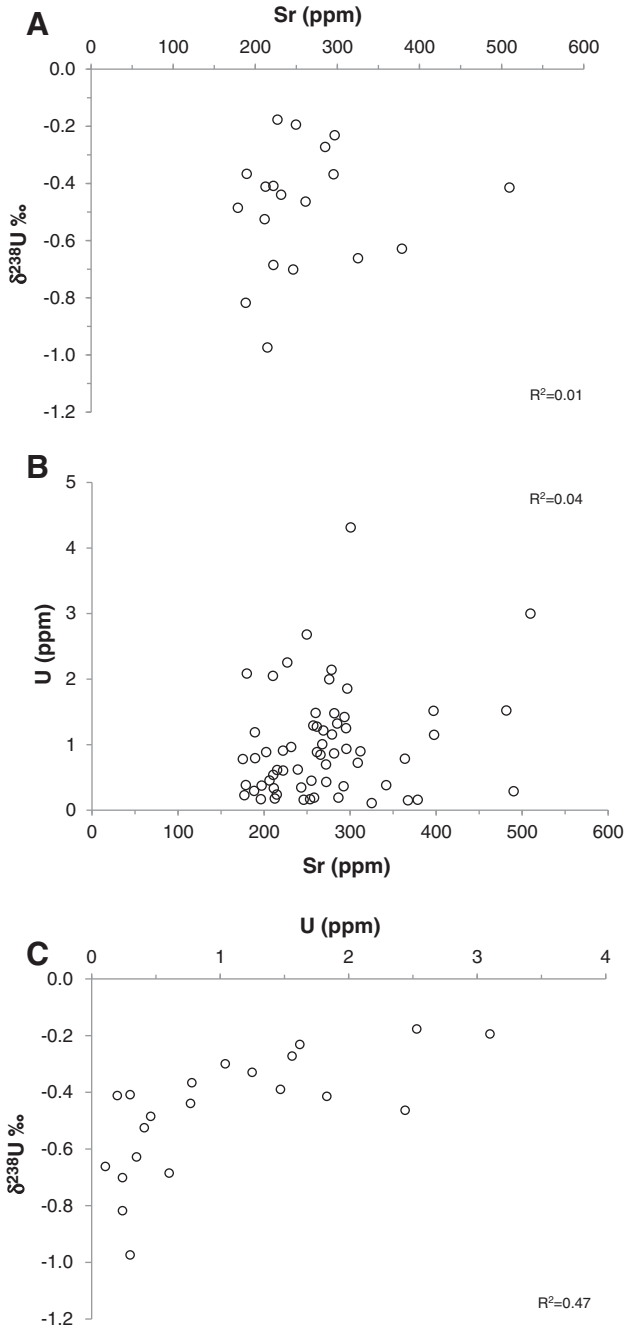

Fig. 7. Scatter diagrams of Sr vs. (A) $\delta^{238}U$, (B) U showing insignificant correlations, and (C) U vs. $\delta^{238}U$. Detail in text.

grain size of the investigated lime mudstone rhythmites argues against significant diagenetic alteration (Azmy et al., 2014). Further evidence against diagenetic alteration is the poor correlation of $\delta^{238}U$ values and also U concentrations with their Sr counterparts (Fig. 7A–B), since Sr is well known to become significantly depleted in altered carbonates with progressive diagenesis (Brand and Veizer, 1980; Veizer, 1983). Similarly, no significant correlations of $\delta^{238}U$ values and U concentrations have been found with other elements such as Al, Si or Ti ($R^2 < 0.1$), which argues against inputs from clastic inclusions and their possible influence on the $\delta^{238}U$ signatures.

The alternation between organic-rich shales and thin carbonate interbeds in the GSSP section in Green Point possibly caused the U to be preferentially enriched in the shales leaving the local seawater depleted, thus leading to deposition of U-depleted carbonates. This may explain the lower U contents of the GSSP lime mudstone rhythmites relative to their modern Bahamas counterparts (Romaniello et al., 2013) and also supports their primary nature. The partial restriction in water circulation and in the basin connection to open ocean water during the interval that spans the geochemical anomaly (Cooper et al., 2001; Azmy et al., 2014), as indicated by disappearance and decrease of diversity of some pelagic organisms (Cooper et al., 2001; Terfelt et al., 2012, 2014; Pouille et al., 2014) immediately above the geochemical anomaly level (Fig. 4; Bed 19 to Bed 24), might have also enhanced the depletion of U in the carbonate rhythmites (i.e., because of slow rates of deep-water renewal in the basin).

On the other hand, the low U contents throughout the investigated section may simply reflect dominantly dysoxic rather than anoxic conditions (Wignall and Twitchett, 1996). Uranium (insoluble U^{+4}) is generally enriched in black shales with the increase in reducing conditions (Wignall and Twitchett, 1996; Montoya-Pino et al., 2010), and similarly in sulfidic marine carbonates of carbonate-dominant environments such as the Bahamas (Romaniello et al., 2013). Given the lack of pyrite (<1%) in the GSSP carbonates, lower amounts of dissolved pore water sulfide may explain the lower U contents of the Green Point carbonates compared to Bahamian carbonates. This observation is relevant to the magnitude of U isotope fractionation between seawater and carbonate sediments. As shown for the Bahamas, strong reducing conditions promoted by high dissolved pore water sulfide concentrations leads to the preferential removal of ^{238}U relative to ^{235}U, resulting in bulk carbonate sediments with $\delta^{238}U$ that is 0.2–0.4‰ higher than seawater (Romaniello et al., 2013). In the case of the Green Point carbonate rhythmites, the lower levels of dissolved sulfide implied by the low U concentrations and pyrite contents suggest that there was a generally smaller isotopic offset between these carbonates and coeval Cambrian–Ordovician seawater compared to that between the Bahamas and modern seawater.

Although a moderate positive correlation is observed between U concentrations and $\delta^{238}U$ in the carbonates ($R^2 = 0.47$, Fig. 7C), the samples with low U concentrations have $\delta^{238}U$ that falls well below the range of detrital compositions ($\delta^{238}U = -0.51$ to -0.20‰; Weyer et al., 2008; Telus et al., 2012). Therefore, input of detrital material is unlikely to be the reason for the variations observed in $\delta^{238}U$, which is consistent with petrographic evidence (lack of siliciclastic inclusions), low Al and Si contents, and lack of covariation between $\delta^{238}U$ and Al, Si, and Ti contents (Appendix 1).

The $\delta^{238}U$ values show an overall decrease upsection to ≤−0.4‰, which is correlated with the negative $\delta^{13}C_{carb}$ excursion and with the increase in $\delta^{15}N_{org}$ values (Fig. 4). The mean $\delta^{238}U$ value (-0.58 ± 0.18‰, Table 1) of the carbonate interbeds above the geochemical anomaly level, which marks the base of the $\delta^{13}C_{carb}$ excursion (Fig. 4), is lower than its counterpart below the anomaly level (-0.28 ± 0.11‰, Table 1) and thus reflects relative depletion in ^{238}U due to sealevel rise (Figs. 2 and 4) and increase in reducing conditions. This change in ocean redox conditions may be widespread because U has a long seawater residence time (~400–500 kyr today; Ku et al., 1977; Dunk et al., 2002) and carbonate $\delta^{238}U$ can reflect global ocean paleoredox conditions (e.g., Brennecka et al., 2011). Below the anomaly, the mean $\delta^{238}U$ value is close to that of modern seawater (-0.40 ± 0.03‰; Weyer et al., 2008; Andersen et al., 2014), taking into account the possibility that the Green Point carbonates are offset to slightly heavier U isotope compositions compared to seawater (Romaniello et al., 2013). Hence, the marine U isotope mass balance and extent of ocean oxygenation before the start of the $\delta^{13}C_{carb}$ excursion may have been similar to the modern ocean.

The insignificant correlation between Al and Th/U ($R^2 = 0.14$) supports the lack of influence of siliciclastic inputs. Although Th/U

ratios are below 2 and reflect dysoxic/reducing conditions throughout the entire investigated boundary section, they show a slight change (~0.2) from a mean value of 0.5 below the geochemical anomaly (Table 1) to 0.7 above the anomaly (Table 1). The drop in the $\delta^{238}U$ values above the anomaly level is correlated with the slight increase in the mean Th/U ratio (Fig. 4 and Table 1). A comparable drop in $\delta^{238}U$ values with a similar rise in the Th/U ratios (~0.2), and also associated with a negative $\delta^{13}C_{carb}$ excursion, has been documented in the Upper Permian GSSP (Brennecka et al., 2011). The low $\delta^{238}U$ in the Upper Permian carbonates is believed to reflect a global expansion in anoxic conditions that caused an increase in the preferential removal of heavy ^{238}U to organic-rich shales, thus driving seawater $\delta^{238}U$ to lighter values (Brennecka et al., 2011). Consistent with the shift to lower $\delta^{238}U$ values, the increase in Th/U ratios suggests a mild decrease in the global seawater U inventory because of a global expansion in the extent of reducing conditions. However, the overall change in the Th/U ratios across the negative $\delta^{13}C_{carb}$ excursion is small (~0.2) relative to the total variation of Th/U ratios in the Cambrian–Ordovician GSSP boundary section, which suggests that its interpretation has to be taken with caution.

In addition to changes in global ocean paleoredox conditions, deposition of the organic-rich shales in the local marine basin may have affected the isotopic composition of U in the alternating thin carbonate beds. A relative increase in the extent of reducing conditions in the marine basin associated with the negative $\delta^{13}C_{carb}$ excursion may have caused an increase in the extent of preferential removal of the heavier ^{238}U isotope from seawater to the organic-rich shales (cf. Weyer et al., 2008; Montoya-Pino et al., 2010; Andersen et al., 2014). Consequently, bottom waters in the basin may have developed lighter $\delta^{238}U$ relative to open ocean seawater, which is reflected in the spatially associated (alternating) carbonate interbeds. The general prevalence of lower $\delta^{238}U$ during the negative $\delta^{13}C_{carb}$ excursion suggests that the implied restriction in the basin connection to the open ocean (Cooper et al., 2001; Azmy et al., 2014) might have contributed to the increase in reducing conditions.

This hypothesis is based on observations of the U isotope variations in the euxinic sediments of the modern Black Sea and Cariaco Basin, which are suggested to be related to the extent of U removal from local bottom waters (Weyer et al., 2008; Montoya-Pino et al., 2010; Andersen et al., 2014). Extensive removal of isotopically heavy U to organic-rich sediments during the GSSP Cambrian–Ordovician boundary interval would lead to bottom waters that are isotopically light and depleted in U, which are then captured by the stratigraphically alternating carbonates. By contrast, a smaller extent of isotopically heavy U removal to organic-rich sediments at a time of less reducing conditions will leave bottom waters that are relatively isotopically heavier and more enriched in U. This process can account for the moderate positive correlation between U concentrations and $\delta^{238}U$ in the Green Point carbonates.

In summary, despite the well-pronounced change in the $\delta^{13}C_{carb}$ profile across the GSSP boundary section, the changes in the TOC, N, $\delta^{15}N_{org}$, and $\delta^{238}U$ counterparts are not similarly sharp. The nature of the local sedimentary environment seems to have some control on those proxies since the investigated carbonates were slope deposits where a dysoxic environment dominated. The rise in sealevel was not accompanied by a dramatic change from locally oxic to anoxic conditions but rather a relative increase in the dysoxic conditions, which is supported by the lack of paleontological evidence for a major extinction event.

7. Conclusions

The slope-setting lime mudstone rhythmites of the Cambrian–Ordovician GSSP boundary section in Green Point (western Newfoundland, Canada) exhibit extensive petrographic preservation and retention of, at least, their near-primary geochemical signatures.

The TOC profile across the boundary shows a drop above a geochemical anomaly level that was marked by the start of a documented negative $\delta^{13}C_{carb}$ excursion. Although the $\delta^{13}C_{org}$ profile does not show a distinct change, the $\delta^{15}N_{org}$ profile exhibits an enrichment correlated with the $\delta^{13}C_{carb}$ excursion, which suggests an increase in the reducing/dysoxic conditions due to sealevel rise.

The $\delta^{238}U$ profile shows a decrease in correlation with the $\delta^{13}C_{carb}$ excursion, thus suggesting an enhancement in the reducing conditions, which is consistent with the $\delta^{15}N_{org}$ results. The rhythmic occurrence of organic-rich shale with thin carbonate interbeds may have influenced the $\delta^{238}U$ signatures of the carbonates.

The Ce/Ce* (0.9 ± 0.1) and Th/U (0.6 ± 0.6) ratios, along with N- and U-isotope results, also support the expansion of relatively more dysoxic conditions in correlation with the documented negative $\delta^{13}C_{carb}$ excursion, which is consistent with the occurrence of phosphatic algae in a few beds. This may imply that the change in redox conditions was most likely not severe enough to cause an extinction event, which is in agreement with the lack of paleontological evidences of major faunal extinction and with the invariable low pyrite contents in the carbonate interbeds throughout the GSSP boundary section.

Acknowledgments

The authors wish to thank Drs. Thierry Corrège (editor), Feng Lu (reviewer) and Ed Landing (reviewer) for their constructive reviews. Also, the efforts of Ms. Krishnaveni Kunchala (Journal manager) are much appreciated. This project was supported by funding (to Karem Azmy) from Petroleum Exploration Enhancement Program (PEEP) (to Brian Kendall) from a NSERC (RGPIN-435930) Discovery Grant, and (to Svend Stouge) from the Carlsberg Foundation (2013_01_0664). Stephen Romaniello is thanked for helpful advice regarding U isotope measurements of carbonates, and Ariel Anbar is thanked for generous access to the W.M. Keck Foundation Laboratory for Environmental Biogeochemistry.

Appendix 1. Elemental and isotopic geochemical compositions of Green Point carbonates. Concentrations of elements are in ppm and all values preceded by the sign "<" are below the detection limit. The column *n* refers to the number of $\delta^{238}U$ measurements for each sample (rpt = replicate sample)

Sample id #	$\delta^{13}C_{carb}$ ‰	$\delta^{18}O$ ‰	$\delta^{13}C_{org}$ ‰	% TOC	$\delta^{15}N_{air}$‰	% N	$\delta^{238}/^{235}U$ ‰	±2σ	$\delta^{234}/^{238}U$ ‰	±2σ	*n*	$CaCO_3$%	$MgCO_3$%	Al	Si	Ti	V	Cr	Mn	Sr
GP 1	−2.26	−7.34	−26.30	2.15	2.08	0.004						97.8	2.2	1539	2586	33	5	2	746	312
GP 2	−1.29	−7.21	−26.97	1.50	1.50	0.003	−0.27	0.04	1.9	1.7	4	98.7	1.3	372	648	19	1	1	800	285
GP 2rpt							−0.30	0.09	5.3	7.9	2									
GP 3	−2.37	−7.22	−28.78	2.56	−0.50	0.061						98.5	1.5	1043	1855	37	4	2	499	215
GP 4	−1.39	−7.09	−26.71	3.35	0.31	0.002						98.8	1.2	540	927	17	2	1	531	301
GP 5	−1.10	−7.25	−26.09	2.21	1.83	0.003						97.9	2.1	1328	1903	27	3	1	489	296
GP 6	−1.07	−7.11	−27.87	1.62	0.67	0.005						98.8	1.2	492	802	18	2	1	315	260
GP 7	−0.32	−6.89	−26.44	4.14	0.99	0.003	−0.46	0.05	0.8	5.5	3	98.8	1.2	520	858	20	2	1	346	261
GP 8	−2.01	−7.72	−27.04	0.99	0.93	0.007						97.0	3.0	1935	2922	48	7	3	483	294
GP 9	−0.67	−7.08	−26.37	2.37	1.83	0.003						98.7	1.3	568	1146	24	2	2	389	266
GP 10	−0.81	−7.56	−29.03	0.97	−0.07	0.011						98.8	1.2	633	1045	18	1	1	579	239
GP 11	−1.49	−5.63	−29.41	2.35	0.10	0.048						62.0	38.0	11,754	17,706	314	176	23	1054	279
GP 12	−1.32	−5.52	−27.58	0.91	−0.31	0.008						63.8	36.2	4902	9331	106	34	8	985	206
GP 13	0.75	−6.87										99.1	0.9	302	462	13	1	1	267	211
GP 14	−1.52	−7.45	−28.92	0.80	−0.55	0.023	−0.18	0.08	28.2	5.2	4	98.7	1.3	878	1366	23	3	2	671	227
GP 15	−1.11	−8.57	−25.73	0.39	1.26	0.006						98.0	2.0	3162	6529	86	4	4	331	490
GP 16	−1.20	−8.53	−26.16	2.42	1.90	0.004						99.0	1.0	647	1117	12	4	1	282	364
GP 17	−1.07	−7.06	−26.37	1.52	4.28	0.003						98.6	1.4	1102	1778	30	3	2	684	210
GP 18	0.36	−6.98	−26.55	2.39	1.90	0.005	−0.23		5.3		1	98.7	1.3	640	999	18	3	1	280	297
GP 19	−0.30	−7.15	−25.63	2.62	1.99	0.004						98.8	1.2	687	1008	17	2	1	435	257
GP 20	0.13	−7.12	−28.17	1.15	2.43	0.003						98.8	1.2	483	879	20	1	1	371	272
GP 21	0.03	−6.98	−27.14	1.81	0.21	0.013						98.8	1.2	489	858	19	2	1	396	276
GP 22	−0.18	−7.09	−28.54	1.62	0.10	0.008	−0.19	0.01	−14.3	1.4	3	98.8	1.2	371	716	15	2	2	369	250
GP 23	0.06	−7.16	−27.64	0.40	2.58	0.003						98.5	1.5	692	1190	24	2	2	579	255
GP 24	0.02	−7.32	−29.20	0.81	−0.06	0.019						98.5	1.5	614	1187	22	2	1	644	282
GP 25	0.36	−7.37	−25.95	0.74	2.08	0.003	−0.37		9.8		1	98.5	1.5	1083	2024	30	3	1	628	190
GP 26	0.27	−7.19	−25.89	1.52	1.47	0.003						97.6	2.4	1558	2712	37	3	2	558	175
GP 27	−2.05	−8.65	−27.34	1.83	3.72	0.021						97.9	2.1	1785	3988	38	9	2	386	510
GP 28	−2.04	−8.37	−27.78	0.83	0.15	0.005	−0.41	0.09	6.3	4.8	3	98.1	1.9	1104	2294	23	5	2	365	482
GP 28rpt							−0.39	0.15	6.7	0.7	4									
GP 29	−4.40	−7.38	−28.38	0.43	2.11	0.007	−0.49	0.10	14.6	5.7	4	98.7	1.3	766	1321	14	1	1	405	179
GP 30	−2.46	−7.37	−28.59	0.44	3.73	0.016	−0.70	0.04	2.3	2.3	3	98.6	1.4	703	1267	15	2	1	376	246
GP 31	−2.75	−7.40	−25.71	1.47	4.16	0.004						98.7	1.3	725	1259	14	1	1	339	196
GP 32	−3.00	−8.02	−28.36	0.16	3.21	2.914						98.6	1.4	686	1158	14	1	1	460	258
GP 33	−1.45	−8.04	−26.37	0.34	3.87	0.641						98.0	2.0	1571	3442	30	4	2	273	397
GP 33A	−4.09	−7.28	−27.66	0.10	1.88	1.471						98.5	1.5	1137	1761	15	2	1	338	197
GP 34	−4.72	−6.98	−26.21	0.27	4.44	0.107	−0.69	0.12	11.2	2.1	4	98.5	1.5	920	1615	20	2	1	325	222
GP 35	−1.03	−6.92	−29.36	0.23	2.60	0.484						98.4	1.6	1188	1724	25	9	1	474	180
GP 36	−1.22	−7.03	−28.66	0.31	2.14	0.585						98.6	1.4	910	1384	29	4	1	249	203
GP 37	−0.62	−6.84										98.3	1.7	1142	1843	16	1	1	193	189
GP 38	0.64	−7.20	−28.75	0.13	2.32	0.026	−0.63	0.09	2.3	5.3	4	98.4	1.6	706	1225	21	1	1	122	379
GP 39	−1.05	−8.04	−29.71	0.43	2.25	0.232						98.5	1.5	1010	1757	20	2	1	273	286

Appendix 1. (*continued*)

Sample id #	$\delta^{13}C_{carb}$ ‰	$\delta^{18}O$ ‰	$\delta^{13}C_{org}$ ‰	% TOC	$\delta^{15}N_{air}$‰	% N	$\delta^{238}/^{235}U$ ‰	±2σ	$\delta^{234}/^{238}U$ ‰	±2σ	*n*	$CaCO_3$%	$MgCO_3$%	Al	Si	Ti	V	Cr	Mn	Sr
GP 40	−3.42	−7.44					−0.97	0.15	7.9	6.3	4	98.7	1.3	745	1217	15	1	1	254	215
GP 40 A	−1.30	−7.29																		
GP 41	−2.57	−7.17	−26.22	0.20	1.97	0.064						97.2	2.8	2010	3827	27	3	3	338	222
GP 41 A	−1.18	−7.11					−0.41	0.02	−2.5	3.7	3	98.7	1.3	579	1169	<0.02	1	1	210	243
GP 42	−0.88	−6.90	−26.98	0.06	4.86	0.009						98.9	1.1	496	1015	<0.02	0	2	288	177
GP 43	1.73	−6.98	−26.98	0.11	5.99	0.007						98.2	1.8	671	1361	15	1	2	94	367
GP 44	1.32	−6.67			1.64							98.2	1.8	473	1094	17	1	2	90	342
GP 45	−0.21	−6.86					−0.82	0.02	−7.3	0.9	3	98.8	1.2	427	884	12	1	1	824	189
GP 46	−3.03	−6.83	−26.31	0.33	3.28	0.003	−0.41		−21.3		1	98.8	1.2	286	520	9	1	2	834	213
GP 47	−4.26	−6.91					−0.53	0.06	−9.4	3.0	3	98.6	1.4	644	1151	14	4	2	385	211
GP 48	−1.02	−7.49	−28.02	0.72	1.60	0.130	−0.44	0.09	8.1	0.6	2	98.1	1.9	1371	2369	35	5	3	449	232
GP 49	−0.34	−7.47										98.6	1.4	230	453	5	2	5	213	398
GP 50	0.56	−7.55	−27.58	0.78	2.26	0.380						98.5	1.5	1064	1822	27	4	4	201	262
GP 51	−0.87	−7.29										98.5	1.5	1036	1727	32	4	4	149	272
GP 52	−2.86	−7.76	−28.12	0.33	4.82	0.048						98.4	1.6	472		16	2	2	178	293
GP 53	0.17	−6.91	−28.12	0.22	4.62	0.093	−0.66	0.11	−20.8	1.7	4	98.7	1.3	406	666	16	2	2	128	325
GP 54	−0.75	−8.12										98.5	1.5	380	672	5	2	2	439	254
GP 55	1.47	−7.12	−26.24	0.26	4.85	0.004						98.7	1.3	783	1282	18	2	2	148	309
GP 56	1.06	−7.40										98.8	1.2	532	973	21	2	3	144	282
GP 57	0.06	−7.92	−28.27	0.36	1.83	0.036						98.8	1.2	677	1047	29	5	3	179	269
GP 58	0.24	−7.46										98.8	1.2	611	1041	30	6	3	200	268
GP 59	0.27	−7.38	−28.97	1.43	0.58	0.514	−0.33	0.13	6.1	5.7	4	98.9	1.1	487	818	25	3	3	129	295
GP 59rpt							−0.37	0.06	4.9	1.2	3									
GP 60	−0.57	−7.60	−28.81	0.85	1.63	0.204						98.9	1.1	690	1288	39	10	4	138	279
GP 61	−0.07	−7.70																		
GP 62	0.07	−7.94	−28.68	2.06	0.12	0.627														
GP 63	−1.76	−7.84	−29.14	1.41	0.90	0.469														
GP 64	−2.04	−7.81	−29.11	4.16	0.37	3.557														
GP 65	−2.25	−7.21																		
GP 66			−29.42	1.88	1.97	1.667														
GP 67	−1.83	−7.72																		
GP 68	−1.06	−7.88																		
GP 69	−1.92	−7.42																		
GP 70	−1.71	−7.42																		
GP 71	−0.33	−7.21																		
GP 72	−1.92	−7.88																		
GP 73	−0.12	−7.72																		
GP 74	0.60	−7.78																		
GP 75	0.81	−7.76																		
GP 76	0.80	−7.79																		
GP 77	0.85	−7.77																		
GP 78	0.66	−7.84																		
GP 79	0.78	−7.85																		
GP 80	0.83	−7.61																		
GP 81	0.57	−7.82																		
GP 82	0.65	−7.78																		

Appendix 1. (*continued*)

Sample id #	Co	Ni	Cu	Mo	P	Y	La	Ce	Pr	Nd	Sm	Eu	Gd	Tb	Dy	Ho	Er	Tm	Yb	Lu	Th	U	Th/U	Y/Ho
GP 1	<0.001	<0.004	<0.003	0.10	209	10	15.699	27.167	2.932	11.027	1.802	0.446	2.011	0.292	1.506	0.309	0.872	0.113	0.720	0.108	0.779	0.897	0.87	31
GP 2	<0.001	<0.004	<0.003	0.17	141	6	8.174	14.288	1.404	5.311	0.880	0.233	1.096	0.149	0.794	0.169	0.486	0.058	0.392	0.059	0.339	1.560	0.26	34
GP 2rpt																						1.040		
GP 3	<0.001	<0.004	<0.003	0.13	88	25	30.057	58.174	5.766	22.516	3.979	1.053	4.842	0.753	4.081	0.845	2.344	0.293	1.772	0.260	0.561	0.612	0.92	29
GP 4	<0.001	<0.004	<0.003	0.05	134	13	15.086	25.171	2.481	9.606	1.692	0.453	2.072	0.310	1.701	0.368	1.024	0.136	0.820	0.125	0.320	4.313	0.07	35
GP 5	<0.001	<0.004	<0.003	0.07	184	10	13.876	24.957	2.820	10.201	1.764	0.459	1.962	0.291	1.470	0.303	0.829	0.111	0.703	0.105	0.588	0.935	0.63	31
GP 6	<0.001	<0.004	<0.003	0.09	73	5	7.706	11.765	1.359	4.813	0.787	0.209	0.888	0.126	0.627	0.123	0.350	0.043	0.267	0.038	0.208	1.483	0.14	41
GP 7	<0.001	<0.004	<0.003	0.07	80	4	5.809	9.617	1.118	4.080	0.701	0.176	0.782	0.111	0.553	0.114	0.302	0.038	0.236	0.033	0.297	2.440	0.23	35
GP 8	<0.001	<0.004	<0.003	0.09	319	17	23.211	42.063	4.829	18.181	3.396	0.863	3.772	0.560	2.917	0.584	1.607	0.206	1.263	0.179	0.937	1.421	0.66	29
GP 9	<0.001	<0.004	14	0.08	101	4	5.543	9.184	1.056	3.953	0.738	0.200	0.821	0.119	0.580	0.113	0.308	0.035	0.207	0.031	0.248	0.844	0.29	35
GP 10	<0.001	<0.004	<0.003	0.09	163	8	16.065	23.233	2.779	9.815	1.692	0.495	1.887	0.276	1.391	0.263	0.683	0.081	0.507	0.072	0.267	0.619	0.43	29
GP 11	18	47	29		868	7	12.687	27.001	3.412	13.090	2.403	0.541	2.385	0.331	1.571	0.298	0.774	0.092	0.565	0.080				
GP 12	46	5	6		586	9	13.439	27.555	3.408	12.884	2.387	0.547	2.427	0.356	1.784	0.345	0.941	0.115	0.724	0.104				
GP 13	<0.001	<0.004	<0.003	0.09	77	2	3.761	5.564	0.623	2.104	0.325	0.083	0.345	0.049	0.235	0.044	0.125	0.015	0.093	0.014	0.151	0.538	0.28	39
GP 14	<0.001	<0.004	<0.003	0.29	90	16	15.313	23.670	2.799	10.890	2.066	0.581	2.487	0.391	2.159	0.452	1.287	0.157	0.926	0.139	0.346	2.530	0.15	34
GP 15	6	<0.004	<0.003	0.28	295	23	26.675	43.883	5.429	19.622	3.736	1.003	3.972	0.688	3.733	0.742	2.112	0.274	1.782	0.256	0.485	0.288	1.68	31
GP 16	<0.001	<0.004	<0.003	0.96	674	34	41.762	68.584	9.009	34.280	6.612	1.823	7.135	1.119	5.488	1.042	2.696	0.308	1.886	0.263	0.480	0.784	0.61	33
GP 17	<0.001	<0.004	<0.003	0.07	106	25	27.513	43.061	4.327	16.364	2.795	0.760	3.608	0.562	3.285	0.738	2.249	0.318	1.987	0.305	0.454	2.047	0.22	33
GP 18	<0.001	<0.004	<0.003	0.09	86	7	10.585	17.976	2.118	7.751	1.294	0.355	1.491	0.209	1.063	0.201	0.566	0.069	0.436	0.062	0.338	1.620	0.18	36
GP 19	<0.001	<0.004	<0.003	0.07	184	11	16.910	31.614	3.356	12.316	2.133	0.550	2.520	0.354	1.905	0.395	1.156	0.152	0.950	0.139	0.310	1.290	0.24	29
GP 20	<0.001	<0.004	<0.003	0.08	96	7	9.389	16.397	1.899	6.941	1.225	0.326	1.418	0.209	1.037	0.194	0.538	0.062	0.398	0.057	0.255	0.697	0.37	35
GP 21	<0.001	<0.004	<0.003	0.19	105	5	7.874	13.628	1.586	5.760	0.977	0.257	1.095	0.152	0.779	0.151	0.406	0.052	0.319	0.046	0.298	1.995	0.15	34
GP 22	<0.001	<0.004	<0.003	0.10	774	7	8.262	14.369	1.726	6.668	1.271	0.332	1.447	0.197	0.967	0.186	0.513	0.062	0.364	0.056	0.220	3.100	0.08	37
GP 23	<0.001	<0.004	<0.003	0.04	203	7	7.867	13.243	1.672	6.404	1.203	0.321	1.380	0.198	1.044	0.205	0.520	0.069	0.421	0.063	0.401	0.448	0.90	35
GP 24	<0.001	<0.004	<0.003	0.23	199	6	9.499	15.173	1.861	6.770	1.300	0.340	1.391	0.192	0.915	0.171	0.440	0.053	0.303	0.045	0.368	1.477	0.25	34
GP 25	<0.001	<0.004	1	0.04	104	14	13.040	20.923	2.479	9.406	1.668	0.457	2.015	0.314	1.786	0.383	1.152	0.159	1.030	0.157	0.469	0.780	0.59	36
GP 26	<0.001	<0.004	<0.003	0.03	111	8	10.773	17.965	2.043	7.270	1.274	0.308	1.377	0.197	1.051	0.222	0.616	0.085	0.502	0.071	0.500	0.779	0.64	35
GP 27	<0.001	<0.004	<0.003	0.26	7914	42	65.134	104.063	13.581	50.121	8.572	2.185	9.303	1.248	5.953	1.161	3.135	0.369	2.119	0.302	1.016	2.998	0.34	36
GP 28	<0.001	<0.004	0	0.41	3061	27	41.753	60.064	7.393	26.268	4.397	1.129	4.836	0.664	3.292	0.646	1.812	0.227	1.383	0.195	0.500	1.830	0.33	42
GP 28rpt																						1.470		
GP 29	<0.001	<0.004	<0.003	0.05	76	7	15.102	21.185	2.180	7.393	1.102	0.280	1.390	0.188	1.023	0.225	0.695	0.096	0.608	0.088	0.228	0.460	0.60	30
GP 30	<0.001	<0.004	<0.003	0.03	98	5	10.816	16.722	1.940	6.754	1.077	0.268	1.188	0.155	0.746	0.149	0.417	0.049	0.317	0.044	0.231	0.240	1.45	34
GP 31	<0.001	<0.004	<0.003	0.04	80	5	13.053	19.796	2.380	8.145	1.262	0.316	1.380	0.169	0.805	0.158	0.423	0.052	0.307	0.044	0.224	0.167	1.34	33
GP 32	<0.001	<0.004	<0.003	0.03	88	8	25.425	34.275	4.239	14.539	2.137	0.599	2.420	0.296	1.297	0.251	0.645	0.074	0.436	0.061	0.219	0.191	1.15	33
GP 33	1	<0.004	5	1.91	4227	20	40.075	60.483	8.162	30.298	5.234	1.436	5.354	0.706	3.146	0.574	1.504	0.160	0.880	0.125	0.659	1.190	0.43	35
GP 33A	<0.001	<0.004	<0.003	0.01	70	6	11.355	18.851	2.112	7.435	1.169	0.279	1.334	0.173	0.836	0.166	0.461	0.056	0.346	0.050	0.187	0.373	0.50	35
GP 34	<0.001	<0.004	<0.003	0.09	115	6	11.060	18.819	2.092	7.407	1.231	0.303	1.345	0.187	0.941	0.200	0.558	0.071	0.459	0.067	0.235	0.603	0.39	30
GP 35	<0.001	<0.004	<0.003	0.20	96	11	17.682	26.695	3.032	11.116	1.874	0.461	2.213	0.304	1.574	0.327	0.931	0.119	0.718	0.107	0.413	2.084	0.20	34
GP 36	<0.001	<0.004	<0.003	0.71	123	5	8.791	13.007	1.621	5.906	0.963	0.228	1.027	0.133	0.658	0.129	0.339	0.042	0.266	0.038	0.347	0.885	0.39	37
GP 37	<0.001	<0.004	<0.003	0.06	104	6	9.381	14.936	1.572	5.696	0.897	0.211	1.048	0.141	0.725	0.146	0.438	0.053	0.338	0.046	0.206	1.187	0.17	42
GP 38	<0.001	<0.004	<0.003	0.10	97	3	6.270	10.162	1.261	4.348	0.663	0.154	0.700	0.089	0.400	0.075	0.215	0.023	0.154	0.021	0.264	0.350	1.67	37
GP 39	<0.001	<0.004	<0.003	0.05	167	6	13.982	19.761	2.258	8.044	1.357	0.332	1.481	0.201	0.969	0.199	0.549	0.066	0.400	0.058	0.190	0.190	1.00	30
GP 40	<0.001	<0.004	<0.003	0.02	90	8	8.824	14.449	1.567	5.800	0.936	0.234	1.104	0.150	0.754	0.154	0.434	0.053	0.310	0.044	0.171	0.300	0.72	53
GP 40 A																								

Appendix 1. (*continued*)

Sample id #	Co	Ni	Cu	Mo	P	Y	La	Ce	Pr	Nd	Sm	Eu	Gd	Tb	Dy	Ho	Er	Tm	Yb	Lu	Th	U	Th/U	Y/Ho
GP 41	<0.001	<0.004	4	0.17	125																	0.908		
GP 41 A	<0.001	<0.004	3	0.21	72																	0.300		
GP 42	<0.001	<0.004	4	0.19	58																	0.227		
GP 43	<0.001	<0.004	4	0.44	95																	0.150		
GP 44	<0.001	<0.004	4	0.34	101																	0.381		
GP 45	<0.001	<0.004	2	0.08	72																	0.240		
GP 46	<0.001	<0.004	2	0.09	112																	0.200		
GP 47	<0.001	<0.004	2	0.17	150																	0.410		
GP 48	<0.001	<0.004	4	0.38	145																	0.770		
GP 49	<0.001	<0.004	3	1.28	582																	1.148		
GP 50	<0.001	<0.004	3	0.74	159																	0.885		
GP 51	<0.001	<0.004	3	0.52	154																	0.429		
GP 52	<0.001	<0.004	3	0.26	334																	0.364		
GP 53	<0.001	<0.004	<0.003	0.19	110																	0.107		
GP 54	<0.001	<0.004	<0.003	0.68	146																	0.167		
GP 55	<0.001	<0.004	<0.003	0.33	122																	0.722		
GP 56	<0.001	<0.004	<0.003	0.81	116																	0.865		
GP 57	<0.001	<0.004	<0.003	0.34	109																	1.215		
GP 58	<0.001	<0.004	<0.003	0.30	115																	1.006		
GP 59	<0.001	<0.004	<0.003	0.62	162																	1.249		
GP 59rpt																								
GP 60	<0.001	<0.004	<0.003	0.47	130																	2.142		
GP 61																								
GP 62																								
GP 63																								
GP 64																								
GP 65																								
GP 66																								
GP 67																								
GP 68																								
GP 69																								
GP 70																								
GP 71																								
GP 72																								
GP 73																								
GP 74																								
GP 75																								
GP 76																								
GP 77																								
GP 78																								
GP 79																								
GP 80																								
GP 81																								
GP 82																								

References

Alibo, D.S., Nozaki, Y., 1999. Rare earth elements in sweater: particle association, shale-normalization, and Ce oxidation. Geochim. Cosmochim. Acta 63 (3–4), 363–372.

Andersen, M.B., Stirling, C.H., Potter, E.K., Halliday, A.N., 2004. Toward epsilon levels of measurement precision on $^{234}U/^{238}U$ by using MC-ICPMS Int. J. Mass Spectrom. 237 (2–3), 107–118.

Andersen, M.B., Romaniello, S., Vance, D., Little, S.H., Herdman, R., Lyons, T.W., 2014. A modern framework for the interpretation of $^{238}U/^{235}U$ in studies of ancient ocean redox. Earth Planet. Sci. Lett. 400, 184–194.

Arnaboldi, M., Meyers, P.A., 2007. Trace element indicators of increased primary production and decreased water-column ventilation during deposition of latest Pliocene sapropels at five locations across the Mediterranean Sea. Palaeogeogr. Palaeoclimatol. Palaeoecol. 249, 425–443.

Asael, D., Tissot, F.L.H., Reinhard, C.T., Rouxel, O., Dauphas, N., Lyons, T.W., Ponzevera, E., Liorzou, C., Chéron, S., 2013. Coupled molybdenum, iron and uranium stable isotopes as oceanic paleoredox proxies during the Paleoproterozoic Shunga Event. Chem. Geol. 362, 193–210.

Azmy, K., Stouge, S., Christiansen, J.L., Harper, D.A.T., Knight, I., Boyce, D., 2010. Carbon-isotope stratigraphy of the Lower Ordovician succession in Northeast Greenland: implications for correlations with St. George Group in western Newfoundland (Canada) and beyond. Sediment. Geol. 225, 67–81.

Azmy, K., Brand, U., Sylvester, P., Gleeson, S., Logan, A., Bitner, M.A., 2011. Biogenic low-Mg calcite (brachiopods): proxy of seawater–REE composition, natural processes and diagenetic alteration. Chem. Geol. 280, 180–190.

Azmy, K., Mottequin, B., Poty, E., 2012. Frasnian–Famenian pre-event: a record from the Dinant Basin, Belgium. Palaeogeogr. Palaeoclimatol. Palaeoecol. 313, 93–106.

Azmy, K., Stouge, S., Brand, U., Bagnoli, G., 2014. High-resolution chemostratigraphy of the Cambrian–Ordovician GSSP in western Newfoundland, Canada: enhanced global correlation tool. Palaeogeogr. Palaeoclimatol. Palaeoecol. 409, 135–144.

Barnes, C.R., 1988. The proposed Cambrian–Ordovician global boundary stratotype and point (GSSP) in western Newfoundland, Canada. Geol. Mag. 125, 381–414.

Bau, M., Dulski, P., 1996. Distribution of yttrium and rare-earth elements in the Penge and Kuruman iron-formations, Transvaal Supergroup, South Africa. Precambrian Res. 79, 37–55.

Brand, U., Veizer, J., 1980. Chemical diagenesis of a multicomponent carbonate system: 1. Trace elements. J. Sediment. Petrol. 50, 1219–1236.

Brand, U., Logan, A., Bitner, M.A., Griesshaber, E., Azmy, K., Buhl, D., 2011. What is the ideal proxy of Paleozoic seawater? Assoc. Australas. Paleontol. Mem. 41, 9–24.

Brennecka, G.A., Herrmanna, A.D., Algeo, T.J., Anbara, A.D., 2011. Rapid expansion of oceanic anoxia immediately before the end-Permian mass extinction. Proc. Natl. Acad. Sci. U. S. A. 108 (43), 17631–17634.

Cawood, P.A., McCausland, P.J.A., Dunning, G.R., 2001. Opening Iapetus: constraints from Laurentian margin in Newfoundland. Geol. Soc. Am. Bull. 113, 443–453.

Çoban-Yıldız, Y., Altabet, M.A., Yılmaz, A., Tuğrul, S., 2006. Carbon and nitrogen isotopic ratios of suspended particulate organic matter (SPOM) in the Black Sea water column. Deep-Sea Res. II 53, 1875–1892.

Condon, D.J., McLean, N., Noble, S.R., Bowring, S.A., 2010. Isotopic composition (U-238/U-235) of some commonly used uranium reference materials. Geochim. Cosmochim. Acta 74 (24), 7127–7143.

Cooper, R.A., Nowlan, G.S., Williams, S.H., 2001. Global stratotype section and point for base of the Ordovician System. Episodes 24, 19–28.

Dahl, T.W., Boyle, R.A., Canfield, D.E., Connelly, J.N., Gill, B.C., Lenton, T.M., Bizzarro, M., 2014. Uranium isotopes distinguish two geochemically distinct stages during the later Cambrian SPICE event. Earth Planet. Sci. Lett. 401, 313–326.

Davies, N.S., Gibling, M.R., 2010. Cambrian to Devonian evolution of alluvial systems: the sedimentological impact of the earliest land plants. Earth-Sci. Rev. 98, 171–200.

Dickson, J.A.D., 1966. Carbonate identification and genesis as revealed by staining. J. Sediment. Petrol. 36, 491–505.

Dickson, A.J., Cohen, A.S., Coe, A.L., 2011. Seawater oxygenation during the Paleocene–Eocene Thermal Maximum. Geology 40 (7), 639–642.

Dunk, R.M., Mills, R.A., Jenkins, W.J., 2002. A reevaluation of the oceanic uranium budget for the Holocene. Chem. Geol. 190, 45–67.

Falkowski, P.G., 2004. Biogeochemistry of primary production in the sea. In: Elderfield, H., Holland, H.D., Turekian, K.K. (Eds.), Biogeochemistry, Treatise on Geochemistry v. 8. Elsevier, Amsterdam, Heidelberg, pp. 185–213.

Faure, G., Mensing, T.M., 2005. Isotopes: Principles and Applications. third edition. John Willey and Sons, Inc., Hoboken, New Jersey (897 pp.).

Fry, B., Jannasch, H.W., Molyneaux, S.J., Wirsen, C.O., Muramoto, J.A., King, S., 1991. Stable isotope studies of the carbon, nitrogen and sulfur cycles in the Black Sea and the Cariaco Trench. Deep-Sea Res. 38, S1003–S1019.

Galbraith, E.D., Sigman, D.M., Robinson, R.S., Pedersen, T.F., 2008. Nitrogen in past marine environments. In: Capone, D.G., Bronk, D.A., Mulholland, M.R., Carpenter, E.J. (Eds.), Nitrogen in the Marine Environment, 2nd edition Academic Press, pp. 1497–1535 (Chapter 34).

Halverson, G.P., Hoffman, P.F., Schrag, D.P., Maloof, A.C., Rice, A.H.N., 2005. Toward a Neoproterozoic composite carbon-isotope record. Geol. Soc. Am. Bull. 117, 1181–1207.

Hatch, J.R., Leventhal, J.S., 1992. Relationship between inferred redox potential of the depositional environment and geochemistry of the Upper Pennsylvanian (Missourian) Stark Shale Member of the Dennis Limestone, Wabaunsee Country, Kansas, U.S.A. Chem. Geol. 99, 65–82.

Herrmann, A.D., Kendall, B., Algeo, T.J., Gordon, G.W., Wasylenki, L.E., Anbar, A.D., 2012. Anomalous molybdenum isotope trends in Upper Pennsylvanian euxinic facies: significance for use of $\delta^{98}Mo$ as a global marine redox proxy. Chem. Geol. 324–325, 87–98.

Hibbard, J.P., van Staal, C.R., Ranking, D.G., 2007. A comparative analysis of pre-Silurian crustal building blocks of the northern and southern Appalachian orogeny. Am. J. Sci. 307, 23–45.

Immenhauser, I., Holmden, C., Patterson, W.P., 2008. Interpreting the carbon-isotope record of ancient shallow epiric seas: lessons from the Recent. In: Pratt, B.R., Holmden, C. (Eds.), Dynamics of Epeiric Seas. Geological Association of Canada, Special Paper 48, pp. 137–174.

James, N.P., Stevens, P.K., 1986. Stratigraphy and correlation of the Cambro-Ordovician Cow Head Group, western Newfoundland. Bull. Geol. Surv. Can. 366, 1–143.

James, N.P., Stevens, R.K., Barnes, C.R., Knight, I., 1989. Evolution of a Lower Paleozoic continental-margin carbonate platform, northern Canadian Appalachians. In: Crevello, P.D., Wilson, J.L., Sarg, J.F., Read, J.F. (Eds.), Controls on Carbonate Platform and Basin Development, Society of Economic Paleontologists and Mineralogists Special Publication 44, pp. 123–146.

Kendall, B., Brennecka, G.A., Weyer, S., Anbar, A.D., 2013. Uranium isotope fractionation suggests oxidative uranium mobilization at 2.50 Ga. Chem. Geol. 362, 105–114.

Kendall, B., Komiya, T., Lyons, T.W., Bates, S.M., Gordon, G.W., Romaniello, S.J., Jiang, G., Creaser, R.A., Xiao, S., McFadden, K., Sawaki, Y., Tahata, M., Shu, D., Han, J., Li, Y., Chu, X., Anbar, A.D., 2015. Uranium and molybdenum isotope evidence for an episode of widespread ocean oxygenation during the late Ediacaran Period. Geochim. Cosmochim. Acta 156, 173–193.

Kimura, H., Azmy, K., Yamamuro, M., Zhi-Wen, J., Cizdziel, J.V., 2005. Integrated stratigraphy of the Upper Proterozoic succession in Yunnan of South China: re-evaluation of global correlation and carbon cycle. Precambrian Res. 138, 1–36.

Knight, I., Azmy, K., Greene, M., Lavoie, D., 2007. Lithostratigraphic setting of diagenetic, isotopic, and geochemistry studies of Ibexian and Whiterockian carbonates of the St. George and Table Head groups in western Newfoundland. Current Research Newfoundland and Labrador Department of Natural Resources Geological Survey. Report 07-1, pp. 55–84.

Knight, I., Azmy, K., Boyce, D., Lavoie, D., 2008. Tremadocian carbonates of the lower St. George Group, Port au Port Peninsula, western Newfoundland: lithostratigraphic setting of diagenetic, isotopic, and geochemistry studies. Current Research Newfoundland and Labrador Department of Natural Resources Geological Survey. Report 08-1, pp. 1–43.

Ku, T.L., Knauss, K., Mathieu, G.G., 1977. Uranium in the open ocean: concentration and isotopic composition. Deep-Sea Res. 24, 1005–1017.

Landing, E., 2007. Ediacaran–Ordovician of east Laurentia—geologic setting and controls on deposition along the New York Promontory. In: Landing, E. (Ed.), Ediacaran–Ordovician of East Laurentia—S. W. Ford Memorial Volume. New York State Museum Bulletin 510, pp. 5–24 (93 p.).

Landing, E., 2012. Time-specific black mudstones and global hyperwarming on the Cambrian–Ordovician slope and shelf of the Laurentia palaeocontinent. Palaeogeogr. Palaeoclimatol. Palaeoecol. 367–368, 256–272.

Landing, E., 2013. The Great American Carbonate Bank in northeast Laurentia: its births, deaths, and linkage to continental slope oxygenation (Early Cambrian–Late Ordovician). In: Derby, J.R., Fritz, R.D., Longacre, S.A., Morgan, W.A., Sternbach, C.A. (Eds.), The Great American Carbonate Bank, Essays in Honor of James Lee Wilson. American Association of Petroleum Geologists Bulletin, Memoir 98, pp. 451–492.

Landing, E., Geyer, G., Bartowski, K.E., 2002. Latest Early Cambrian small shelly fossils, trilobites, and Hatch Hill dysaerobic interval on the east Laurentian continental slope. J. Paleontol. 76, 285–303.

Landing, E., Keppie, J.D., Westrop, S.R., 2007. Terminal Cambrian and lowest Ordovician of Mexican West Gondwana—biotas and sequence stratigraphy of the Tiñu Formation. Geol. Mag. 144, 909–936.

Lavoie, D., Desrochers, A., Dix, G., Knight, A., Hersi, O.S., 2013. The great carbonate Bank in eastern Canada: an overview. In: Derby, J., Fritz, R., Longcare, S., Morgan, W., Sternbach, C. (Eds.), The Great American Carbonate Bank: The Geology and Economic Resources of Cambrian–Ordovician Sauk Megasequence of Laurentia. American Association of Petroleum Geologists, Memoir 98, pp. 499–524.

Lécuyer, C., Grandjean, P., Barrat, J.-A., Nolvak, J., Emig, C., Paris, F., Robardet, M., 1998. $\delta^{18}O$ and REE contents of phosphatic brachiopods: a comparison between modern and lower Paleozoic populations. Geochim. Cosmochim. Acta 62, 2429–2436.

Lehnert, O., Miller, J.F., Leslie, S.A., Repetski, J.E., Ethington, R.L., 2005. Cambro-Ordovician sea-level fluctuations and sequence boundaries: the missing record and evolution of new taxa. Spec. Pap. Palaeontol. 73, 117–134.

Machel, H.G., Burton, E.A., 1991. Factors governing cathodoluminescence in calcite and dolomite, and their implications for studies of carbonate diagenesis. Luminescence Microscopy and Spectroscopy, Qualitative and Quantitative Applications. SEPM Short Course 25, pp. 37–57.

Meyers, P.A., 1994. Preservation of elemental and isotopic source identification of sedimentary organic matter. Chem. Geol. 144, 289–302.

Montoya-Pino, C., Weyer, S., Anbar, A.D., Pross, J., Oschmann, W., van de Schootbrugge, B., Arz, H.W., 2010. Global enhancement of ocean anoxia during Oceanic Anoxic Event 2: a quantitative approach using U isotopes. Geology 38, 315–318.

Morel, F.M.M., Milligan, A.J., Saito, M.A., 2004. Marine bioinorganic chemistry: the role of trace metals in the oceanic cycles of major nutrients. In: Elderfield, H., Holland, H.D., Turekian, K.K. (Eds.), The Oceans and Marine Geochemistry, Treatise on Geochemistry volume 6. Elsevier, Amsterdam, Heidelberg, pp. 113–143.

Murphy, A.E., Sageman, B.B., Hollander, D.J., Lyons, D.J., Brett, C.E., 2000. Black shale deposition and faunal overturn in the Devonian Appalachian basin: clastic starvation, seasonal water-column mixing, and efficient biolimiting nutrient recycling. Paleoceanography 15, 280–291.

Piper, D.Z., Calvert, S.E., 2009. A marine biogeochemical perspective on black shale deposition. Earth Sci. Rev. 95, 63–96.

Popp, B.N., Parekh, P., Tilbrook, B., Bidigare, R.R., Laws, E.A., 1997. Organic carbon $\delta^{13}C$ variations in sedimentary rocks as chemostratigraphic and paleoenvironmental tools. Palaeogeogr. Palaeoclimatol. Palaeoecol. 132, 119–132.

Pouille, L., Danelian, T., Maletz, J., 2014. Radiolarian diversity changes during the Late Cambrian–Early Ordovician transition as recorded in the Cow Head Group of Newfoundland (Canada). Mar. Micropaleontol. 110, 25–41.

Quan, T.M., van de Schootbrugge, B., Field, M.P., Rosenthal, Y., Falkowski, P.G., 2008. Nitrogen isotope and trace metal analyses from the Mingolsheim core (Germany): evidence for redox variations across the Triassic–Jurassic boundary. Glob. Biogeochem. Cycles 22, GB2014.

Quan, T.M., Wright, J.D., Falkowski, P.G., 2013. Co-variation of nitrogen isotopes and redo states through glacial–interglacial cycles in the Black Sea. Geochim. Cosmochim. Acta 112, 305–320.

Romaniello, S.J., Herrmann, A.D., Anbar, A.D., 2013. Uranium concentrations and $^{238}U/^{235}U$ isotope ratios in modern carbonates from the Bahamas: assessing a novel paleoredox proxy. Chem. Geol. 362, 305–316.

Rush, P.F., Chafetz, H.S., 1990. Fabric retentive, non-luminescent brachiopods as indicators of original $\delta^{13}C$ and $\delta^{18}O$ compositions: a test. J. Sediment. Petrol. 60, 968–981.

Śliwiński, M.G., Whalen, M.T., Day, J., 2010. Trace element variations in the Middle Frasnian punctata zone (Late Devonian) in the western Canada sedimentary Basin—changes in oceanic bioproductivity and paleoredox spurred by a pulse of terrestrial afforestation? Geol. Belg. 4, 459–482.

Telus, M., Dauphas, N., Moynier, F., Tissot, F.L.H., Teng, F.-Z., Nabelek, P.I., Craddock, P.R., Groat, L.A., 2012. Iron, zinc, magnesium and uranium isotopic fractionation during continental crust differentiation: the tale from migmatites, granitoids, and pegmatites. Geochim. Cosmochim. Acta 97, 247–265.

Terfelt, F., Bagnoli, G., Stouge, S., 2012. Re-evaluation of the conodont *Iapetognathus* and implications for the base of the Ordovician System GSSP. Lethaia 45, 227–237.

Terfelt, F., Eriksson, M.E., Schmitz, B., 2014. The Cambrian–Ordovician transition in dysoxic facies in Baltica—diverse faunas and carbon isotope anomalies. Palaeogeogr. Palaeoclimatol. Palaeoecol. 394, 59–73.

Theissen, K.M., Dunbar, R.B., Cooper, A.K., 2003. Stable isotopic measurements of sedimentary organic matter and *N. Pachyderma* (S.) from Site 1166, Prydz Bay continental shelf. In: Cooper, A.K., O'Brien, P.E., Richter, C. (Eds.), Proceedings of the Ocean Drilling Program, Scientific Results 188, pp. 1–11.

Tribovillard, N., Algeo, T.J., Lyons, T., Riboulleau, A., 2006. Trace metals as paleoredox and paleoproductivity proxies: an update. Chem. Geol. 232, 12–32.

Veizer, J., 1983. Chemical diagenesis of carbonates. In: Arthur, M.A., Anderson, T.F., Kaplan, I.R., Veizer, J., Land, L.S. (Eds.), Theory and Application of Trace Element Technique, Stable Isotopes in Sedimentary Geology. Society of Economic Paleontologists and Mineralogists (SEPM) Short Course Notes 10, pp. III-1–III-100.

Veizer, J., Ala, D., Azmy, K., Bruckschen, P., Bruhn, F., Buhl, D., Carden, G., Diener, A., Ebneth, S., Goddris, Y., Jasper, T., Korte, C., Pawellek, F., Podlaha, O., Strauss, H., 1999. $^{87}Sr/^{86}Sr$, $\delta^{18}O$ and $\delta^{13}C$ evolution of Phanerozoic seawater. Chem. Geol. 161, 59–88.

Verbruggen, A., Alonso, A., Eykens, R., Kehoe, F., Kuhn, H., Richter, S., Aregbe, Y., 2008. Preparation and Certification of IRMM-3636, IRMM-3636a, and IRMM-3636b. Institute for Reference Materials and Measurements (27 p.).

Weaver, F.J., Macko, S.A., 1988. Source rocks of western Newfoundland. Org. Chem. 13 (1–3), 411–421.

Webb, G.E., Kamber, B.S., 2000. Rare Earth elements in Holocene reefal microbialites: a new shallow seawater proxy. Geochim. Cosmochim. Acta 64 (9), 1557–1565.

Weyer, S., Anbar, A.D., Gerdes, A., Gordon, G.W., Algeo, T.J., Boyle, E.A., 2008. Natural fractionation of $^{238}U/^{235}U$. Geochim. Cosmochim. Acta 72, 345–359.

Wignall, P.B., Twitchett, R.J., 1996. Oceanic anoxia and the end Permian mass extinction. Science 272, 1155–1158.

Wignall, P.B., Zonneveld, J.-P., Newton, R.J., Amor, K., Sephton, M.A., Hartley, S., 2007. The end Triassic mass extinction record of Williston Lake, British Columbia. Palaeogeogr. Palaeoclimatol. Palaeoecol. 253, 385–406.

Wilson, J.L., Medlock, P.L., Fritz, R.D., Canter, K.L., Geesaman, R.G., 1992. A review of Cambro-Ordovician breccias in North America. In: Candelaria, M.P., Reed, C.L. (Eds.), Paleokarst, Karst-related Diagenesis and Reservoir Development. SEPM—Permian Basin Section, Publication 92-33, pp. 19–29.

Yamaguchi, K.E., Ogurim, K., Ogawa, N.O., Sakai, S., Hirano, S., Kitazato, H., Ohkouchi, N., 2010. Geochemistry of modern carbonaceous sediments overlain by a water mass showing photic zone anoxia in the saline meromictic Lake Kai-ike, southwest Japan: I. Early diagenesis of organic carbon, nitrogen, and phosphorus. Palaeogeogr. Palaeoclimatol. Palaeoecol. 294, 72–82.

Zhou, L., Wignall, P.B., Su, J., Feng, Q., Xie, S., Zhao, L., Huang, J., 2012. U/Mo ratios and $\delta^{95}/^{95}Mo$ as local and global redox proxies during mass extinction events. Chem. Geol. 324–325, 99–107.